This is the accepted version of a paper published in *IEEE Transactions on Cybernetics*. This paper has been peer-reviewed but does not include the final publisher proof-corrections or journal pagination.

Access to the published version may require subscription.

N.B. When citing this work, cite the original published paper.

A Multilateral Teleoperation System: New Cooperative Structure based on Reconfigurable Robot Hand and Controller Design based on Type-2 Fuzzy Model

Da Sun, Qianfang Liao, Xiaoyi Gu, Changsheng Li and Hongliang Ren

Abstract – This paper develops an innovative multilateral teleoperation system with two haptic devices in the master side and a newly-designed reconfigurable multi-fingered robot hand in the slave side. A novel non-singular fast terminal sliding mode (NFTSM) algorithm together with varying dominance factors for cooperation is proposed to offer this system fast position and force tracking, as well as an integrate perception for the operator on the robot hand. Type-2 fuzzy model is used to describe the overall system dynamics, and accordingly a new fuzzy-model-based state observer is proposed to compensate for the system uncertainties. A sliding mode adaptive controller is designed to deal with the varying zero drift of the force sensors and force observers. The stability of the closed-loop system under time-varying delays is proved using Lyapunov-Krasovskii functions. Finally, experiments to grasp different objects are performed to verify the effectiveness of this multilateral teleoperation system.

Index terms – Multilateral teleoperation, Multi-fingered robot hand, Sliding mode control, Type-2 T-S Fuzzy Logic

1. Introduction

In recent years, robot hands have been undergoing ascending tendency in substituting human hands and executing various tasks in considerable areas. The existing robot hands can be classified into different types based on the stiffness and actuation mode. The high stiffness of the rigid robot hand will make the full actuation undesirable for friendly human/environmental robotic interaction [1]-[2]. Additionally, complex mechanical structures and sophisticated control algorithms are required to achieve precise control of the position and the output force, the costs of fabricating and maintaining these robot hands could be extremely high. On the other hand, the robot hands based on soft materials, e.g. silicon gel and fabric, and pneumatic/hydraulic actuation have unique advantage in compatibility and safety because of their low stiffness, which attracting progressive attention and interest of robotic researchers and engineers [3]-[4]. Nevertheless, loading capability, robustness, and controllability are serious issues that prevent the practical application of this technology.

Corresponding authors: Qianfang Liao

Da Sun (ds744@uowmail.edu.au) and Qianfang Liao (qfliao1@e.ntu.edu.sg) are with Center for Applied Autonomous Sensor System, Örebro universitet, Sweden.

Xiaoyi Gu (e0019922@u.nus.edu), Changsheng Li (lics32@163.com) and Hongliang Ren (ren@nus.edu.sg) are with Department of Biomedical Engineering, National University of Singapore, Singapore.

Combining the advantages of the above mentioned two robotic hands, underactuated robotic hands, which are mostly based on the cable-driven mechanism, have the intrinsic compliance as well as the soft robot hands [5]-[6], but enhanced loading capability, improved robustness, and better controllability. While compared to fully actuated robot hands, underactuated robotic hands have moderate stiffness and better compatibility. Additionally, they are generally having simpler structures and thus with greatly reduced cost. In this paper, we focus on the robot hand based on underactuated mechanism, as well as the concept of reconfigurable modular design, which is, the number of modules in each finger and the locations of the fingers can be easily adjusted to meet different requirements. This study aims to develop a new human-involved multilateral teleoperation system to manipulate this robot hand to perform different tasks.

Bilateral and multilateral tele-robotic systems have emerged as a valuable tool that can involve human operator's decision to improve the performance by feeding the remote position and force information back to the human side, and can provide more flexibility than the fully-automated systems. In contrast to the unilateral teleoperation, a well-designed bilateral or multilateral teleoperation system can be characterized by *three aspects*: first, accurate position synchronization of multiple robots; and second, which is more important, reasonable force feedback that allows the operator to have a good perception on the remote environmental object; last but not least, having accurate dynamic models for the robots that can enhance the system performance and meanwhile be supportive for stability achievement.

For the first aspect, numerous studies have been dedicated to the area of multi-robot motion synchronization and the area of dealing with time delays [55]-[56]. Among them, the sliding mode control (SMC) algorithms have proved to largely enhance the transient-state control performance. SMC was introduced in [7]-[8] and was surveyed in [9] in detail. In recent years, SMC is deeply explored in [43]-[45] for the applications of electric vehicles, power systems, chaotic systems and a new second order SMC algorithm is designed to solve the motion problems for single manipulator [10]. Later, SMC on manipulator control is improved in [46] and is extended to the cooperative robotic systems [11]. In order to derive more precise and faster convergence performances, the terminal sliding mode control (TSMC) methods are proposed to guarantee the finite time convergence performance [12], different from the classical linear sliding mode (LSM) that can only provide asymptotical convergence [13]. In the work reported in [14] and [15], a globally continuous non-singular TSMC is proposed as an indirect approach, to deal with the singularity problem. A new non-singular fast terminal sliding

mode (NFTSM)-based teleoperation system combined with fuzzy logic control to enhance the position tracking [16]. Later, this approach is improved by adding synchronization error constraint [17]. Nevertheless, the above teleoperation systems could only maintain stability in the presence of constant time delays. In [18], an NFTSM-based teleoperation system is designed that could be used under time-varying delays by adding additional buffers to keep the delays constant. However, such a method can increase the overall time delays and is hard to pre-set.

In addition, the biggest drawback of the above mentioned NFTSM-based teleoperation systems is that they do not consider force tracking, which means they cannot live up to the standard given in the aforementioned second aspect. Therefore, although fine position tracking is achieved, their operator can hardly make a reasonable decision since no accurate perception on the remote environment can be received, and the end effector of the slave may not exert desired forces on the object, which may cause unexpected consequents. A number of studies introduced the force control method into teleoperation control such as the four-channel teleoperation [19]-[21] and the passivity-based teleoperation [22]. However, they regard the human and environmental impedances as constants with known coefficients or the systems are assumed to be linear with known dynamics, which are against reality. Several force control methods are also applied in the nonlinear teleoperation system by adding the square of force tracking errors [23]-[24] or using dynamic model-based force observer [25]-[27]. Only using force tracking errors with a constant gain as force controllers, these approaches have no superiority on fast convergence of human and environmental forces.

Besides, in plenty of robot applications, the accurate mathematical functions to describe the system dynamics are difficult to achieve, which is an obstacle in developing teleoperation control. In order to meet the standard in the aforementioned third aspect of a good multilateral teleoperation system, fuzzy logic model composed by a batch of "IF-THEN" fuzzy rules can be used as the alternative because: i). fuzzy models are the universal approximators and can be built using input-output data samples or expert experience [28]-[30]; ii). fuzzy system is well known for its strong ability to deal with noises and disturbances [31]. In this paper, the interval Type-2 Takagi-Sugeno (T-S) fuzzy model [35] is chosen to describe the dynamics for the tele-robotic system. Different from the traditional (Type-1) fuzzy model using crisp numbers as the fuzzy memberships, the interval Type-2 fuzzy model uses intervals instead such that it offers additional design degrees to describe the inexactness and thus can increase the robustness. T-S is the name for one of the two most popular structures of fuzzy systems. It is using a group of linear local models blended by fuzzy memberships to describe a global nonlinear system. Compared to the other structure called Mamdani, T-S fuzzy model requires less fuzzy rules and offers a platform to apply the powerful conventional linear algorithms on nonlinear systems [31]. Currently, Type-2 fuzzy logic in the forms of both Mamdani and T-S can be found in a number of studies for control algorithm [44]-[49]. However, few papers use Type-2 T-S fuzzy logic to estimate the robotic uncertainty issues.

Especially in the area of teleoperation system, only a few methods using Type-1 Mamdani fuzzy model based algorithms for robotic system control can be found at present [32]-[34], which gives authors the inspiration to explore advanced methods using more sophisticated fuzzy model.

The main contribution of this paper is developing a novel multilateral teleoperation system where a new cooperative structure is applied on the reconfigurable multi-figured robot hand and a Type-2 fuzzy model based controller is designed to make this human-involved multi-robotic system measure up to the aforementioned three standards. The robot hand in the slave side is self-designed with proper modular structure and locking mechanism for four fingers. The number of modules can be quickly and conveniently adjusted according to specific requirements, and any fractured module can be replaced with a new one without additional tools or breaking driven cables. Moreover, the workspace and stiffness can also be reconfigured, giving significant improvements on both the grasping performance and the versatility of the designed robotic hand. Two haptic devices are used in the master side to collaboratively control the slave robot hand where the four fingers can be considered as two grippers through a new NFTSM algorithm with effective cooperative structure using varying dominance factors. This algorithm not only guarantees finite-time master-slave position tracking performance but also provides reasonable force tracking which allow the robot hand to hold the environment object with adaptive forces and simultaneously let the operator have a mixed perception on the two remote grippers. Type-2 T-S fuzzy model is identified to describe the overall dynamics of each robot and accordingly, a new fuzzy-model-based state observer is proposed to compensate for the dynamic uncertainties. In addition, a new sliding mode adaptive controller is proposed to deal with the varying zero drift of the force sensors and force observers. Lyapunov functions are applied to prove the finite-time stability of the proposed teleoperation system. Finally, a series of grasping experiments are conducted to validate the performance of this multilateral teleoperation system.

2. Design of the tele-manipulated robot hand

As shown in Fig.1 (a) and (b), each module of the robotic finger consists of 6 components. Two main parts of one module mutually connect with each other using a bearing and a 3mm shaft. The bending motion of one modular is achieved by pulling a nylon cord that through the main part 1. The elastic cord with one end fixed to the main part 1 and the other end fixed to the main part 2 facilitates the module to return to its original position. Each module has a separate elastic cord and the stiffness of the joint of one module can be easily adjusted by changing the tightness of the elastic cord. One module is connected to the other with a dovetail groove (Fig.1 (c)). For each finger, only one nylon cord is applied to achieve the bending motion.

As illustrated in Fig. 2, the complete robotic hand system is composed of a few modular designed fingers, a base with several dovetail grooves, two driving shafts, and two servo motors (MX64R, Dynamixel,). Fingers connects to the base using the same connection mode as shown in Fig. 1(c). Nylon

cords used to bend fingers are wrapped around the driving shafts. Each driving shaft, which is rotated and controlled by a servo motor, is capable of actuating at most a pair of fingers. Fig.2 depicts the ability of this robotic hand to reconfigure workspace and stiffness. To pick up tiny objects, e.g. coins, each finger has only one module as shown in Fig. 2 (b). In this condition, this pair of fingers is fully actuated and the robotic hand works as a clamp with high stiffness. To grasp objects with larger size or fragile characteristics, the number of the module of fingers can be easily increased because of the concept of modular design as shown in Fig. 2 (c). Since the actuation mode of the finger with more than one modular is under-actuation, the robotic hand with these fingers have moderate stiffness and is able to achieve a better compatibility. In most cases, two pairs of fingers coordinating with each other are believed to be able to enhance the grasping ability of the robotic hand. In this design, the location of the finger can be easily rearranged. If the object has a regular shape, two pairs of fingers have the same location as shown in Fig. 2 (a) and (e). If the object has an irregular shape, e.g. a wine bottle with a thick body and a thin bottle neck, two pairs of fingers should be placed in a staggered manner as shown in Fig.2(d). Therefore, the reconfigurability of the workspace and stiffness of the robotic hand can be easily realized.
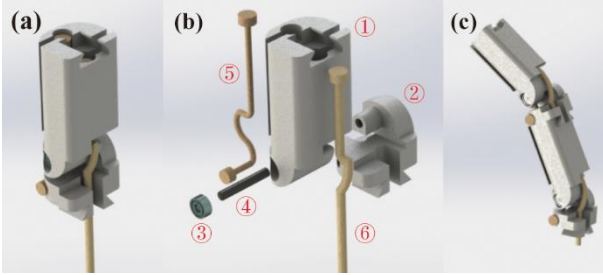

Fig. 1. CAD model of one modular of the finger. (a) Assembly diagram (b) Exploded view. (c) Connection mode. ① Main part 1. ② Main part 2. ③ Bearing. ④ 3mm shaft. ⑤ Elastic cord. ⑥Nylon cord.
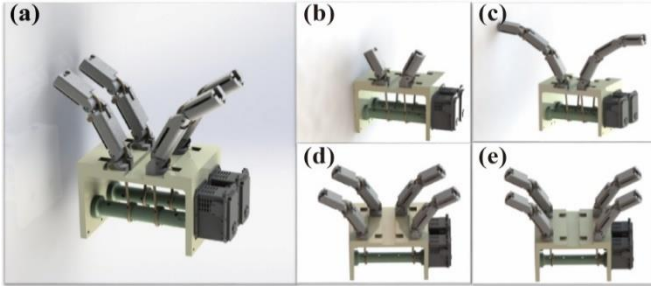

Fig. 2. CAD model of the robotic hand. (a). Robotic hand with two pairs of fingers having the same location. (b). Robotic hand with a pair of fingers, each has one module. (c). Robotic hand with a pair of fingers, each has three modules. (d). Robotic hand with two pair of fingers having the staggered location. (e). Robotic hand with two pair of fingers having the same location.

Fig. 3 shows the diagram of the tele-manipulated robot hand. Two haptic devices are taken as the master 1 and master 2, which can be installed at different places (with different communication delays). For the slave side, since the robot hand consists of two grippers (each gripper contains a pair of fingers), it can be regarded as one integral, or two separates (slave 1 and slave 2). For the forward control, the control signals from master 1 and master 2 are used to control slave 1 and slave 2, respectively. Moreover, in order to offer the robotic hand flexibility to perform remote task, control laws

are also set between the two slave grippers to enhance the mutual cooperation ability. For the backward control, the robotic hand is considered as an integral, and the control signals mixed with the dynamics of the two slave grippers are fed back to the master sides so that the operators of master 1 and master 2 can have the same perception on the remote robot hand, which is conducive for cooperation of the two masters and the motion synchronization of overall system can be improved. From Figs. 1 and 2, one can see that the motors of the proposed robot hand drive the cables in order to control multiple fingers. Therefore, the motors are always loaded even during the free motion condition (the grippers do not contact to any object). If without an accurate estimation of the system dynamics, the uncertainties especially like the external load may seriously degrade the teleoperation system's performance. Accordingly, the Type-2 T-S fuzzy algorithm is introduced in next section.
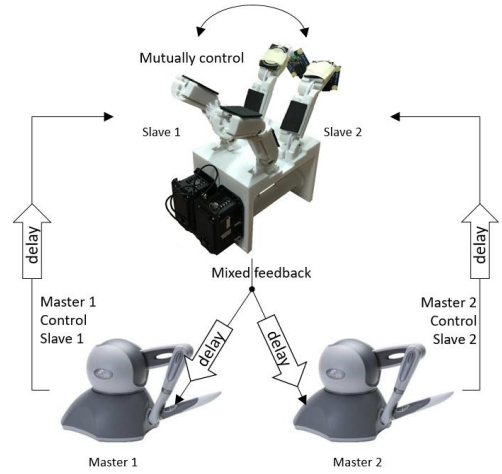

Fig. 3. Diagram of the tele-manipulated robot hand

3. Type-2 T-S fuzzy logic based dynamic models

Notation: An interval vector $\tilde{A} \in R^n$ is composed of n intervals as: $\tilde{A} = [\tilde{A}_1 \cdots \tilde{A}_n]^T$ where $\tilde{A}_i = [\underline{A}_i, \overline{A}_i]$, $\tilde{A}$ can also be expressed as $\tilde{A} = [\underline{A}, \overline{A}]$ where $\underline{A} = [\underline{A}_1 \cdots \underline{A}_n]^T \in R^n$ and $\overline{A} = [\overline{A}_1 \cdots \overline{A}_n]^T \in R^n$.

The dynamics of the master/slave can be described by the following equation:

$$M_i(q_i)\ddot{q}_i + C_i(q_i, \dot{q}_i)\dot{q}_i + g_i(q_i) + f_i\dot{q}_i + f_{ci}(\dot{q}_i) + F_i^d = \tau_i + \tau_j \quad (1)$$

where $i = m1, m2, s1, s2$ represents masters 1 and 2, slave grippers 1 and 2, and $j = h1, h2, e1, e2$ indicates human and environment. $\ddot{q}$, $\dot{q}$, $q \in R^n$ stand for the vectors of joint acceleration, velocity and position signals, respectively. $M_i(q_i) \in R^{n \times n}$ and $C_i(q_i, \dot{q}_i) \in R^{n \times n}$ are the inertia matrices and Coriolis/centrifugal effects, respectively. $g_i(q_i) \in R^n$ is the gravitational force. $f_i\dot{q}_i \in R^n$ and $f_{ci}(\dot{q}_i) \in R^n$ denote the viscous friction and Coulomb friction, respectively. $F_i^d \in R^n$ contains the unknown disturbance and measurement noise. $\tau = [\tau_1 \cdots \tau_n]^T \in R^n$ are control variables, and $\tau_j \in R^n$ is the external human or environmental torques that $\tau_j = \tau_j^* + \Delta\tau_j$, where τ_j^* is the measured torque and $\Delta\tau_j$ is the bounded measurement error.

Remark 1: An accurate equation (1) for a robotic system is generally difficult to derive. T-S fuzzy model is a solution for this problem since it can be built to a high degree of accuracy based on data samples and human experience [28]-[29]. In addition, powerful conventional linear methods can be applied on T-S fuzzy model since it is composed of a batch of linear local models, and fuzzy control is a robust tool to deal with noise and disturbance [29]. This paper takes interval Type-2 T-S fuzzy model as an alternative to the mathematical function in (1). Interval Type-2 T-S fuzzy model utilizes intervals instead of crisp numbers as the fuzzy membership grades and local models' coefficients which possessing increased power to describe uncertainties [35].

The fuzzy rules used to describe the dynamics of n-DOF robotic system is in the following form:

Rule l ($l = 1, \cdots, L$):
IF $x(k)$ is $\tilde{Z}^l$, THEN $C_i^l v_i(k) + D_i^l q_i(k) + \tilde{E}_i^l = \tilde{\tau}_i^l(k)$ (2)

where L is the number of fuzzy rules; $x(k) = [v(k)^T \ q(k)^T]^T \in R^{2n}$, $v_i(k) \in R^n$ and $q_i(k) \in R^n$ are velocity and position signals at time k; $\tilde{Z}^l$ is an interval Type-2 fuzzy set in which $x(k)$'s fuzzy membership is an interval denoted by $\tilde{\mu}^l(x(k)) = [\underline{\mu}^l(x(k)), \ \overline{\mu}^l(x(k))]$, $\underline{\mu}^l(x(k))$ and $\overline{\mu}^l(x(k))$ are lower and upper bounds, respectively; $C_i^l \in R^{n \times n}$ and $D_i^l \in R^{n \times n}$ are coefficient matrices; $\tilde{E}_i^l = [\underline{E}_i^l, \ \overline{E}_i^l] \in R^n$ and $\tilde{\tau}_i^l(k) = [\underline{\tau}_i^l(k), \ \overline{\tau}_i^l(k)] \in R^n$ are interval vectors. The local model of (2) can be rewritten by:

$$\begin{cases} \underline{\tau}_i^l(k) = C_i^l v(k) + D_i^l q(k) + \underline{E}_i^l \\ \overline{\tau}_i^l(k) = C_i^l v(k) + D_i^l q(k) + \overline{E}_i^l \end{cases} \quad (3)$$

Blending the L fuzzy rules through fuzzy membership grades achieves a type-reduced set for output, which is also an interval vector $\tilde{\tau}_i(k) = [\underline{\tau}_i(k), \ \overline{\tau}_i(k)]$ derived by:

$$\begin{cases} \underline{\tau}_i(k) = \frac{\sum_{l=1}^L \underline{\mu}^l(x(k)) \times \underline{\tau}_i^l(k)}{\sum_{l=1}^L \underline{\mu}^l(x(k))} = \sum_{l=1}^L \underline{\omega}_i^l(x(k)) \times \underline{\tau}_i^l(k) \\ \overline{\tau}(k) = \frac{\sum_{l=1}^L \overline{\mu}^l(x(k)) \times \overline{\tau}_i^l(k)}{\sum_{l=1}^L \overline{\mu}^l(x(k))} = \sum_{l=1}^L \overline{\omega}_i^l(x(k)) \times \overline{\tau}_i^l(k) \end{cases} \quad (4)$$

where $\underline{\omega}_i^l(x(k)) = \underline{\mu}^l(x(k))/\sum_{l=1}^L \underline{\mu}^l(x(k))$ and $\overline{\omega}_i^l(x(k)) = \overline{\mu}^l(x(k))/\sum_{l=1}^L \overline{\mu}^l(x(k))$. Denote $\omega_i^l(x(k)) = \frac{\overline{\omega}_i^l(x(k)) + \underline{\omega}_i^l(x(k))}{2}$ and $\Delta\omega_i^l(x(k)) = \frac{\overline{\omega}_i^l(x(k)) - \underline{\omega}_i^l(x(k))}{2}$. The dynamics of the robotic system can be expressed by:

$$C_i(k)v_i(k) + D_i(k)q_i(k) + E_i(k) + \lambda(k)\Delta E_i(k) = \tau_i(k) + \tau_j(k) \quad (5)$$

where $\lambda(k) \in [-1, 1]$ is time-varying and unknown, $C_i(k) = \sum_{l=1}^L [\omega_i^l(x(k)) + \lambda(k)\Delta\omega_i^l(x(k))] \times C_i^l$, $D_i(k) = \sum_{l=1}^L [\omega_i^l(x(k)) + \lambda(k)\Delta\omega_i^l(x(k))] \times D_i^l$, $E_i(k) = \frac{\sum_{l=1}^L \overline{\omega}_i^l(x(k)) \times \overline{E}_i^l + \sum_{l=1}^L \underline{\omega}_i^l(x(k)) \times \underline{E}_i^l}{2}$, $\Delta E_i(k) = \frac{\sum_{l=1}^L \overline{\omega}_i^l(x(k)) \times \overline{E}_i^l - \sum_{l=1}^L \underline{\omega}_i^l(x(k)) \times \underline{E}_i^l}{2}$. $\lambda(k)\Delta E_i(k)$ denotes the uncertainties with known bounds. Since the sampling time for

robotic system is sufficiently small, (5) can be regarded as a continuous equation as:

$$C_i \dot{q}_i + D_i q_i + E_i + \lambda \Delta E_i = \tau_i + \tau_j \quad (6)$$

A Type-2 T-S fuzzy model can be identified from input-output data and human experience. Based on a batch of data samples denoted by $z(k) = [x(k)^T \ \tau_i(k)]^T$, $k = 1, \cdots, N$, N is the number of samples, firstly, Gustafson-Kessel clustering algorithm [36] is used to locate L fuzzy set centres, denoted by $z_c^l = [(x_c^l)^T \ \tau_c^l]^T$, $l = 1, \cdots, L$, and to derive a fuzzy partition matrix $U = [\mu^l(z(k))]_{L \times N}$ where $\mu^l(z(k)) \in [0,1]$ is a crisp fuzzy membership grade for $z(k)$ in Rule l and satisfying $\sum_{l=1}^L \mu^l(z(k)) = 1$. Afterwards, using the elements of U as the weights, a linear model for Rule l can be identified using weighted least square algorithm:

$$C_i^l v_i(k) + D_i^l q_i(k) + E_i^l = \tau_i^l(k) \quad (7)$$

Now a traditional Type-1 T-S fuzzy model is derived, and its output can be expressed by the following equation:

$$\sum_{l=1}^L \mu^l(x(k))\left(C_i^l v_i(k) + D_i^l q_i(k) + E_i^l\right) = \\ \sum_{l=1}^L \mu^l(x(k))\tau_i^l(k) = \tau_{T1\_i}(k) \quad (8)$$

where $\tau_{T1\_i}(k)$ denotes the Type-1 fuzzy model's output.

The root-mean-square-error (RMSE) of the model is: $RMSE = \sqrt{\sum_{k=1}^N \left(\tau_{T1\_i}(k) - \tau_i(k)\right)^2 / N}$. The RMSE can be used to determine the number of fuzzy sets/fuzzy rules L. Given an initial small value to L, and a tolerance value ε_{RMSE}, if $RMSE > \varepsilon_{RMSE}$, then let $L = L + 1$, and repeat the above procedure to derive a new Type-1 fuzzy model. When $RMSE \le \varepsilon_{RMSE}$, stop the repeating and go to the next step that extending Type-1 to Type-2.

For the antecedent part of the fuzzy rules, choose a blurring radius $\Delta\mu^l \ge 0$ for fuzzy membership grades in each fuzzy set to achieve Type-2 fuzzy membership grades $\tilde{\mu}^l(z(k))$ by extending $\mu^l(z(k))$ to an interval:

$$\begin{cases} \underline{\mu}^l(z(k)) = \max(\mu^l(z(k)) - \Delta\mu^l, \ 0) \\ \overline{\mu}^l(z(k)) = \min(\mu^l(z(k)) + \Delta\mu^l, \ 1) \end{cases} \quad (9)$$

For the consequent part of the fuzzy rules, choose a $\Delta E_i^l = [\Delta E_{i1}^l \ \cdots \ \Delta E_{in}^l]^T$ where $\Delta E_i^l \ge 0$ ($i = 1, \cdots, n$) for each rule to extend E_i^l in (7) to an interval $\tilde{E}_i^l$:

$$\begin{cases} \underline{E}_i^l = E_i^l - \Delta E_i^l \\ \overline{E}_i^l = E_i^l + \Delta E_i^l \end{cases} \quad (10)$$

The values of $\Delta\mu^l$ and ΔE_i^l can be derived using gradient descent algorithm based on the N collected data samples:

$$\begin{cases} \Delta\mu^l(k+1) = \Delta\mu^l(k) - \eta_\mu \frac{\partial e_\tau}{\partial \Delta\mu^l} \\ \Delta E^l(k+1) = \Delta E^l(k) - \eta_E \frac{\partial e_\tau}{\partial \Delta E^l} \end{cases} \quad (11)$$

where η_μ and η_E are learning coefficients; $e_y = [\tau_{T2\_i}(k) - \tau_i(k)]^2 / 2$, $\tau_{T2\_i}(k)$ denotes Type-2 fuzzy model's output and is calculated by (5) setting $\lambda(k) = 0$. The

calculations of $\partial e_\tau / \partial \Delta \mu^l$ and $\partial e_\tau / \partial \Delta E^l$ are introduced in [37].

When giving a new input vector $x(k)$ to the model, L crisp fuzzy membership grades can be calculated using the distances between $x(k)$ and the centres x_c^l:

$$\mu^l(x(k))$$
$$= \begin{cases} 0, & \overset{v=1,\ldots,L}{\underset{v \neq l}{\forall}} \|x(k) - x_c^v\| = 0 \\ 1, & \|x(k) - x_c^l\| = 0 \\ \dfrac{1}{\sum_{v=1}^{L} \dfrac{\|x(k) - x_c^l\|}{\|x(k) - x_c^v\|}}, & \|x(k) - x_c^v\| \neq 0, for\, v = 1, \ldots, L \end{cases}$$

Afterwards, $\mu^l(x(k))$ can be extended to an interval $\tilde{\mu}^l(x(k))$ according to (9) by replacing $z(k)$ with $x(k)$, and then the output can be calculated by (3)-(5).

4. Multilateral Teleoperation System

4.1. Cooperative Structure based on Non-Singular Fast Terminal Sliding Mode Algorithm

Definition 1: define $sig(\eta)^\alpha$, as:

$$sig(\eta)^\alpha \triangleq [|\eta_1|^{\alpha_1} sign(\eta_1), \ldots, |\eta_n|^{\alpha_n} sign(\eta_n)]^T$$

where $\eta = [\eta_1, \ldots, \eta_n]^T \in R^n$, $\alpha_{1\ldots n}$ are positive constants. $Sign(\cdot)$ is the standard signum function.

Lemma 1: Assume $a_1 > 0$, $a_2 > 0, \ldots,$ $a_n > 0$, if $0 < c < 1$, then $(\alpha_1 + \cdots + \alpha_n)^c \leq \alpha_1^c + \cdots + \alpha_n^c$. If $1 < c < \infty$, then $(\alpha_1 + \cdots + \alpha_n)^c \leq n^{c-1}(\alpha_1^c + \cdots + \alpha_n^c)$.

Lemma 2: (reaching time): consider the dynamic model $\dot{x} = f(x), f(0) = 0$ and $x \in R^n$. If there is a positive definite function $V(x)$ such that $\dot{V}(x) \leq -\mathbb{R}V(x)^{\rho_1} - \mathbb{Z}V(x)^{\rho_2}$ where $\mathbb{R}, \mathbb{Z} > 0$, $\rho_1 > 1$, $0 < \rho_2 < 1$. Then the system is finite-time stable, Furthermore, the settling time is given by $T_r < \frac{1}{\mathbb{R}} \frac{1}{\rho_1 - 1} + \frac{1}{\mathbb{Z}} \frac{1}{1 - \rho_2}$

Lemma 3: (sliding time of the FTSM in [38]) Choose the terminal sliding mode as $s = \dot{e} + \alpha sig(e)^{\gamma_1} + \beta sig(e)^{\gamma_2}$. The convergence time T_s of e is $T_s = \int_0^{|e(0)|} \frac{1}{\alpha x^{\gamma_1} + \beta x^{\gamma_2}} de < \frac{1}{\alpha} \frac{1}{\gamma_1 - 1} + \frac{1}{\beta} \frac{1}{1 - \gamma_2}$ where $\alpha, \beta > 0$, $\gamma_1 > 1$, $0 < \gamma_2 < 1$.

Note that for the above FTSM, the singularity problem often exists. It is because during the process of the derivation of s, $x^{\gamma_2 - 1}$ can cause singularity $s = 0$, $\dot{x} = 0$, but $x \neq 0$. [39]-[40] design a NFTSM control algorithm by adding a new online switching controller to switch the sliding surface from TSM to LSM. However, such approach may cause discontinuity.

In this work, we propose a new sliding surface that aims to have faster convergence time than that of the FTSM in **Lemma 3.** The new sliding surface is designed as

$$s = k_1 sig^{\varphi_1}(e) + k_2 sig^{\varphi_2}(e) + k_3 sig^{\varphi_3}(\dot{e}) \quad (12)$$

where $k_1, k_2, k_3, \varphi_1, \varphi_3$ are positive constants that $k_1, k_2, k_3 > 0$, $\varphi_1 = l_1/p, 1 < \varphi_3 = \frac{l_2}{p} < 2$. l_1, l_2, p are positive odd integer satisfying $l_1 > l_2 > p$. φ_2 is defined as

$$\varphi_2(t) = \frac{\varpi}{\|e\|}, \quad \varpi_1 \leq \frac{\varpi}{\|e\|} \leq \varpi_2 \quad (13)$$

ϖ, ϖ_{1-2} are positive constants and satisfy $0 < \varpi_1 < 1 < \varpi_2$, $0 < \varpi \ll 1$. When e decrease to ϖ, φ_2 can increase from ϖ_1 to 1; and if φ_2 continue to decrease to zero, φ_2 will increase from 1 to ϖ_2.

It follows from (12) that $sign(e) = -sign(\dot{e})$ and $k_3|\dot{e}|^{\varphi_3} = k_1|e|^{\varphi_1} + k_2|e|^{\varphi_2}$. Therefore, (12) can be rewritten as $\dot{e} = -\frac{1}{k_3}^{\frac{1}{\phi_3}} sig^{\frac{1}{\phi_3}}(k_1 e^{\phi_1} + k_2 e^{\phi_2})$. The convergence time of (12) can be expressed as:

$$T_{s1} = \int_0^{|e(0)|} \frac{1}{\left(\frac{k_1}{k_3} e^{\phi_1} + \frac{k_2}{k_3} e^{\phi_2}\right)^{\frac{1}{\phi_3}}} de \quad (14)$$

Consider $\frac{k_1}{k_3} = \alpha$, $\frac{k_2}{k_3} = \beta$, $\phi_1 = \gamma_1$, $\phi_2 = \gamma_2$. Since e is converging to zero, by tuning k_1, k_2, k_3 to guarantee $\frac{k_1}{k_3} e^{\phi_1} + \frac{k_2}{k_3} e^{\phi_2} < 0$, T_{s1} can be guaranteed to be smaller than T_s. From (14), T_{s1} can be derived as:

$$T_{s1} < \left(\frac{k_3}{k_1}\right)^{\frac{1}{\phi_3}} \frac{1}{\frac{\phi_1}{\phi_3} - 1} |e(0)|^{1 - \frac{\phi_1}{\phi_3}} + \left(\frac{k_3}{k_2}\right)^{\frac{1}{\phi_3}} \frac{1}{1 - \frac{\varpi_1}{\phi_3}} |e(0)|^{1 - \frac{\varpi_1}{\phi_3}} \quad (15)$$

When applied to the practical dual-master-dual-slave system, (12) can be re-expressed as $s_i = k_{i1} sig^{\varphi_1}(e_i) + k_{i2} sig^{\varphi_2}(e_i) + k_{i3} sig^{\varphi_3}(e_{vi})$

Remark 2: The forward and backward time delays between master 1 and the slave grippers are $T_{f1}(t)$ and $T_{b1}(t)$, respectively; and those between master 2 and the slave grippers are $T_{f2}(t)$ and $T_{b2}(t)$. The differentials of $T_{f1}(t)$, $T_{f2}(t)$, $T_{b1}(t)$, and $T_{b2}(t)$ are bounded by positive constants $\bar{d}_{f1}$, $\bar{d}_{f2}$, $\bar{d}_{b1}$, $\bar{d}_{b2}$, respectively, which is, $0 \leq |\dot{T}_{f,b-1,2}(t)| \leq \bar{d}_{f,b-1,2}$. Since the main focus of this study is reconfigurable robot hand design and the relevant control logic design for grasping, the large and sharply varying delays are not considered in this paper. For more information about guaranteeing system stability under large and sharply varying delays, please refer to [50]-[54].

We define the position convergence errors e_i as

$$e_{m1}(t) = q_{m1}(t) - D_1(t) q_{s1}(t - T_{b1}(t)) - D_1^-(t) q_{s2}(t - T_{b1}(t))$$
$$e_{m2}(t) = q_{m2}(t) - D_2(t) q_{s1}(t - T_{b2}(t)) - D_2^-(t) q_{s2}(t - T_{b2}(t))$$
$$e_{s1}(t) = q_{s1}(t) - q_{m1}(t - T_{f1}(t))$$
$$e_{s2}(t) = q_{s2}(t) - q_{m2}(t - T_{f2}(t)) \quad (16)$$

where $D_{1,2}(t)$ $D_{1,2}^-(t)$ are the variable dominance factors defined by

$$D_1(t) = \frac{1}{2} tanh\left(\alpha|\tau_{e1}^*(t - T_{b1}(t))| - \alpha|\tau_{e2}^*(t - T_{b1}(t))|\right) + \frac{1}{2}$$
$$D_2(t) = \frac{1}{2} tanh\left(\alpha|\tau_{e1}^*(t - T_{b2}(t))| - \alpha|\tau_{e2}^*(t - T_{b2}(t))|\right) + \frac{1}{2}$$
$$D_1^-(t) = 1 - D_1(t), \qquad D_2^-(t) = 1 - D_2(t) \quad (17)$$

where α is a positive constant. The dominance factors $D_1(t)$ and $D_2(t)$ are varying between 0 to 1 based on the measured environmental torque τ_{e1}^* and τ_{e2}^* satisfying

$$\begin{cases} D_{1,2} > D_{1,2}^- & if \ |\tau_{e1}^*| > |\tau_{e2}^*| \\ D_{1,2} = D_{1,2}^- & if \ |\tau_{e1}^*| = |\tau_{e2}^*| \\ D_{1,2} < D_{1,2}^- & if \ |\tau_{e1}^*| < |\tau_{e2}^*| \end{cases}$$

Accordingly, $D_{1,2}$ can determine the weights of the feedback signals from each slave gripper to the masters. By applying the proposed dominance factors, the operator in the master side can have an integrate perception for the slave robot hand.

Then, define the velocity convergence error e_{vi} as

$$e_{vm1}(t) = \dot{q}_{m1}(t) - D_1(t)\left(1 - \hat{d}_{b1}(t)\right)\dot{q}_{s1}\left(t - T_{b1}(t)\right) - D_1^-\left(1 - \hat{d}_{b1}(t)\right)\dot{q}_{s2}\left(t - T_{b1}(t)\right)$$

$$e_{vm2}(t) = \dot{q}_{m2}(t) - D_2(t)\left(1 - \hat{d}_{b2}\right)\dot{q}_{s1}\left(t - T_{b2}(t)\right) - D_2^-\left(1 - \hat{d}_{b2}\right)\dot{q}_{s2}\left(t - T_{b2}(t)\right)$$

$$e_{vs1}(t) = \left(\dot{q}_{s1}(t) - \left(1 - \hat{d}_{f1}\right)\dot{q}_{m1}\left(t - T_{f1}(t)\right)\right)$$

$$e_{vs2}(t) = \left(\dot{q}_{s2}(t) - \left(1 - \hat{d}_{f2}\right)\dot{q}_{m2}\left(t - T_{f2}(t)\right)\right) \quad (18)$$

where $\hat{d}_{f,b-1,2}$ denote the estimation of $\dot{T}_{f,b-1,2}$ to be introduced later. Accordingly, the sliding time T_{s1} in (14) can be re-expressed as

$$T_{s1-i} = \int_0^{|e(0)|} \frac{1}{\left(\left(\frac{k_{i1}}{k_{i3}}e_i^{\phi_1} + \frac{k_{i2}}{k_{i3}}e_i^{\phi_2}\right)^{\frac{1}{\phi_3}} + \xi_i\right)} de_i \quad (19)$$

where ξ_i are expressed as $\xi_{m1} = D_1(\dot{T}_{b1} - \hat{d}_{b1})\dot{q}_{s1}(t - T_{b1}) + D_1^-(\dot{T}_{b1} - \hat{d}_{b1})\dot{q}_{s2}(t - T_{b1}) - \dot{D}_1 q_{s1}(t - T_{b1}) - \dot{D}_1^- q_{s1}(t - T_{b1})$, $\xi_{m2} = D_2(\dot{T}_{b2} - \hat{d}_{b2})\dot{q}_{s1}(t - T_{b2}) + D_2^-(\dot{T}_{b2} - \hat{d}_{b2})\dot{q}_{s2}(t - T_{b2}) - \dot{D}_2 q_{s1}(t - T_{b2}) - \dot{D}_2^- q_{s2}(t - T_{b2})$, $\xi_{s1} = (\dot{T}_{f1} - \hat{d}_{f1})\dot{q}_{m1}(t - T_{f1})$, $\xi_{s2} = (\dot{T}_{f2} - \hat{d}_{f2})\dot{q}_{m2}(t - T_{f2})$. According to the function and the mechanism structure of the designed gripper, the robot forces are not changing sharply so that $\dot{D}_{1,2}$ and $\dot{D}_{1,2}^-$ are neighbouring zero. Under the condition that the rates of time delays are accurately estimated, ξ_i can be neighboring zero and the sliding time T_{s1-i} is equal to T_{s1} in (14). When the rate of the time delays is inaccurately estimated, T_{s1-i} will be enlarged accordingly.
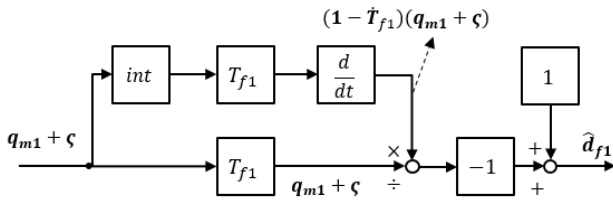

Fig.4. Time delay rate estimator

The time delay rate estimator is designed as Fig.4, where ς is a positive constant satisfying $\varsigma > \max|q_{m1}|$ that can avoid singularity. Noticing that $\frac{dx}{dt} = \frac{x(t^+)-x(t)}{T_{sample}}$ may enlarge noises, we apply the following adaptive law to derive $\frac{dx}{dt}$

$$\dot{y} = b_1(x - y) + b_2(x - y) + b_1 b_2 \int_0^t (x(\iota) - y(\iota))d\iota \quad (20)$$

where b_1 and b_2 are positive gain and $y \rightarrow \frac{dx}{dt}$.

4.2. Type-2 Fuzzy Model based Control Laws

Define the torque tracking errors e_{ti} to be

$$e_{tm1}(t) = \tau_{h1}'(t) - D_1(t)\tau_{e1}'\left(t - T_{b1}(t)\right) - D_1^-\tau_{e2}'\left(t - T_{b1}(t)\right)$$

$$e_{tm2}(t) = \tau_{h2}'(t) - D_2(t)\tau_{e1}'\left(t - T_{b2}(t)\right) - D_2^-\tau_{e2}'\left(t - T_{b2}(t)\right)$$

$$e_{ts1}(t) = \left(\tau_{h1}'\left(t - T_{f1}(t)\right) - \tau_{e1}'(t)\right) + (\tau_{e2}' - \tau_{e1}')$$

$$e_{ts2}(t) = \left(\tau_{h2}'\left(t - T_{f2}(t)\right) - \tau_{e2}'(t)\right) + (\tau_{e1}' - \tau_{e2}') \quad (21)$$

Remark 3: In the practical application, since the human input forces and the sensed environmental contact forces are bounded, tracking errors e_{ti} in (21) are also bounded. Accordingly, we assume e_{ti} are bounded by the known positive constants h_i as $e_{ti} \leq h_i$.

Meanwhile, knowing that the varying zero drift is one of the main problems faced by almost all the force/torque observers and sensors due to the unknown uncertainties or mechanical errors. To compensate for the zero drift, we design the following sliding mode adaptive control algorithm to derive the output τ_j' from the force/torque observers and sensors :

$$\tau_j' = \tau_j^* - d_i \quad (22)$$

where

$$d_i = \begin{cases} -\eth_{i1}d_i + \eth_{i2}sig^{\varphi_1}(\tau_j') + \eth_{i3}sig^{\varphi_2}(\tau_j'), & if \tau_j^* \geq a \\ 0, & else \end{cases} \quad (23)$$

where $\eth_{i1}$, $\eth_{i2}$ and $\eth_{i3}$ are constant control gains. a is a known upper bound of the varying zero drift neighboring zero. When $\tau_j^* \geq a$, the d_i will take effect to force τ_j' fast converge to zero in a finite time by using the predefined sliding mode control algorithm.

For the feedback force controller design, the following adaptive force control algorithm is considered:

$$\epsilon_i = c_{i1}sig^{\varphi_1}(e_{ti}) + c_{i2}sig^{\varphi_2}(e_{ti}) \quad (24)$$

where c_{i1}, c_{i2} are positive constant gains. φ_2 denotes that in (13) by replacing e to e_{ti}. Also, define the adaptive controllers z_i as

$$z_i = sig^{\varphi_1}(y_i) + sig^{\varphi_2}(y_i)$$

$$\dot{y}_i = -p_{i1}(sig^{2\varphi_1-1}(y_i) + sig^{2\varphi_2-1}(y_i)) - p_{i2}\kappa_i\epsilon_i \quad (25)$$

where

$$\kappa_i = \begin{cases} 1, \\ if \ (y_i(t)\epsilon_i(t) > 0) \ || \ (y_i(t)\epsilon_i(t) = 0, y_i(t)\epsilon_i(t^-) \leq 0) \\ -1, \\ if \ (y_i(t)\epsilon_i(t) < 0) \ || \ (y_i(t)\epsilon_i(t) = 0, y_i(t)\epsilon_i(t^-) > 0) \end{cases}$$

$$(26)$$

From (6), the system dynamics can be reformatted as follows:

$$C_i\dot{e}_i + D_ie_i = \tau_i + \tau_j^* + C_i(e_{vi} - \dot{q}_i) + D_i(e_i - q_i) - E_i + G_i \quad (27)$$

where G_i denotes the uncertainties satisfying $G_i = \Delta\tau_j + \xi_i - \Delta E_i$.

Define $Z_i = e_i$, $Z_i^* = G_i/C_i$, (27) can be rewritten as:

$$\begin{cases} \dot{Z}_i = -C_i^{-1}D_iZ_i + Z_i^* \\ +C_i^{-1}(\tau_i + C_i(e_{vi} - \dot{q}_i) + D_i(e_i - q_i) - E_i + \tau_j^*) \\ \dot{Z}_i^* = \omega_i \end{cases} \quad (28)$$

where ω_i denotes the derivatives of the system dynamic uncertainties. Based on (28), the designed adaptive estimator that is used to estimate and compensate for the uncertainties of each robot is written as (29).

$$\begin{cases} \dot{Y}_{i1} = Y_{i2} - C_i^{-1}D_iZ_i + C_i^{-1}(\tau_i + C_i(e_{vi} - \dot{q}_i) \\ +D_i(e_i - q_i) + \tau_j^*) - \beta_{i1}R_i(S_{i1}) - \beta_{i2}S_{i1} \\ \dot{Y}_{i2} = -\beta_{i3}sig(S_{i1})^{\phi_2} \end{cases} \quad (29)$$

where β_{i1}, β_{i2}, β_{i3} are constant gains. Y_{i1}, Y_{i2} are the outputs of the adaptive controller. C_i and D_i are the estimated fuzzy-based dynamics derived from (5). The approximation errors are given as:

$$S_{i1} = Y_{i1} - Z_i, S_{i2} = Y_{i2} - Z_i^* \quad (30)$$

S_{i1}, S_{i2} are expected to converge to zero so that the output Y_{i2} can track the dynamic uncertainty Z_i^*. $\beta_{i3}sig(S_{i1})^{\phi_2}$ yields a high gain when the estimated error is small. To force S_{i1} fast converge to zero with the its upper boundary close to zero at the steady state, S_{i1} is required to be

$$p_iA_i(t) < S_{i1}(t) < p_iA_i(t) \quad (31)$$

where $0 < p_i < 1, \kappa_i > 0$, and the function $A_i(t)$ is defined as:

$$A_i(t) = (A_{i0} - A_{i\infty})e^{-\iota t} + A_{i\infty} \quad (32)$$

where A_{i0}, $A_{i\infty}$ and ι are positive constants; and A_{i0}, the predefined maximum overshoot, is the initial value of the function $A_i(t)$. i.e. $A_{i0} = A_i(0)$. The constant $A_{i\infty} = lim_{t\to\infty}A_i(t)$ is the predefined final small constraint of $A_i(t)$. Also, ι is the convergence velocity, and $0 < \iota < 1$. $R_i(.)$ is a smooth, strictly increasing function shown as

$$R_i(S_{i1}) = tan(\frac{\pi S_{i1}}{2A_i(t)p_i}) \quad (33)$$

The function R_i satisfies: $R_i: (-A_i, A_i) \to (-\infty, +\infty)$. When ϵ_i converges to zero, S_{i1} will also converge to zero, by properly set the convergence velocity ι and the steady-state overshoot $A_{i\infty}$. From (28)-(29), we can derive:

$$\begin{cases} \dot{S}_{i1} = S_{i2} - \beta_{i1}R_i(S_{i1}) - \beta_{i2}S_{i1} \\ \dot{S}_{i2} = -\beta_{i3}sig(S_{i1})^{\phi_2} - \omega_i \end{cases} \quad (34)$$

During the steady state with $\dot{S}_{i1} = 0$, $\dot{S}_{i2} = 0$, (34) can be expressed as:

$$\begin{cases} |S_{i2}| = \beta_{i1}R_i(|\omega_i/\beta_{i3}|^{1/\phi_2}) + \beta_{i2}|\omega_i/\beta_{i3}|^{1/\phi_2} \\ |S_{i1}| = |\omega_i/\beta_{i3}|^{1/\phi_2} \end{cases}$$

By selecting β_{i3} to be large enough, S_{i1} can be guaranteed to be small. As analysed, $R_i(.)$ can force S_{i1} to be bounded by a small value $A_{i\infty}$ and fast converge to zero so that the S_{i2} can be neighbouring zero in the steady state.

This means that Y_{i1} and Y_{i2} are guaranteed to be neighbouring Z_i and Z_i^*, respectively.

The overall control laws for the proposed system are designed as:
$$\tau_i = -b_{i1}sig^{2-\varphi_3}(s_i) - b_{i2}sig^{\varphi_3}(s_i) - e_i + \phi\Gamma_isign(e_i)k_{i3}^{2-\varphi_3}\left|e_{vi}^{\varphi_3(2-\varphi_3)}\right| + \phi\Gamma_isign(e_i)k_{i3}^{\varphi_3}\left|e_{vi}^{\varphi_3^2}\right| + b_{i3}|z_i|\epsilon_i - b_{i4}z_i - C_i(e_{vi} - \dot{q}_i) - D_i(e_i - q_i) - \tau_j^* + D_ie_i + E_i - \hat{G}_i$$
$$(35)$$

where b_{i1}, b_{i2}, b_{i3}, b_{i4} are positive constant gains. $\hat{G}_i = C_iY_{i2}$. Γ_i is designed as

$$\Gamma_i = -sign(sign(e_i)sign(e_{vi})) \quad (36)$$

The control laws in (35) have three aspects:

1). Position tracking controllers: $-b_{i1}sig^{2-\varphi_3}(s_i) - b_{i2}sig^{\varphi_3}(s_i) - e_i + \phi\Gamma_isign(e_i)k_3^{2-\varphi_3}\left|e_{vi}^{\varphi_3(2-\varphi_3)}\right| + \phi\Gamma_isign(e_i)k_3^{\varphi_3}\left|e_{vi}^{\varphi_3^2}\right|$. For slaves, the NFTSM-based controllers allow slave 1 and slave 2 to closely follow the motion of master 1 and master 2, respectively. For masters, according to the definition of position errors in (16), each master robot follows the weighted position of the two slave grippers. Since we see the two slave grippers as an integral part of the overall slave robot, the weighted position can be seen as the position of the whole slave robot. Since each slave gripper closely tracks each master and the two masters uniformly follows the weighted position of the slave robot, accurate motion synchronization can be achieved by the overall multilateral teleoperation systems.

2). Force/torque tracking controllers: $b_{i3}|z_i|\epsilon_i - b_{i4}z_i$. For slaves, the force applied by each slave gripper is not only required to follow that applied by the operator, but needs to be automatically tuned by the force from another gripper to the extent that equal forces can be applied by the two grippers to hold the environmental object with different structures. For masters, each master receives equivalent weighted force signals from the overall slave robot (containing the two grippers) such that operator(s) can feel the same feedback force when driving the two masters.

3). Controllers $-C_i(e_{vi} - \dot{q}_i) - D_i(e_i - q_i) - \tau_j^* + D_ie_i + E_i - \hat{G}_i$ are applied to compensate for the system uncertainties and to guarantee the system stability. The total block diagram is shown as Fig.5.
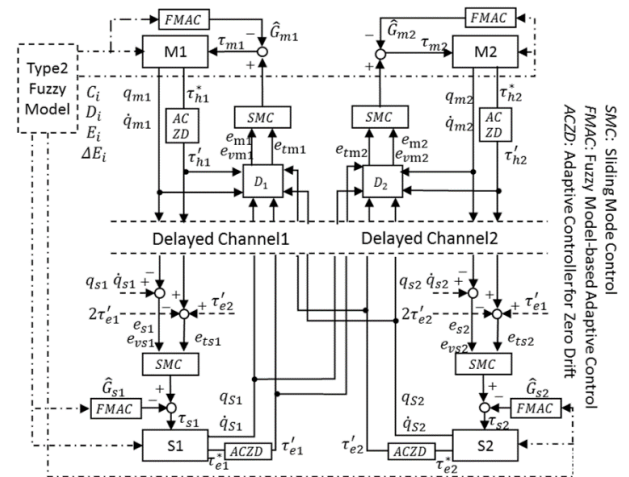

Fig. 5. Total block diagram

5. Stability Analysis

This section analyses the performance and stability of the proposed system. **Theorem 1** proves that in the free space movement without external forces ($\tau_h(t) = \tau_e(t) = 0$), the position synchronization errors can converge to zero in a finite time. **Theorem 2** proves that when human and environmental forces are applied into the system, the system can still remain stable. Moreover, the measured torque errors can be restricted in a pre-defined boundary and converge to zero when time tends to infinity. These two theorems aim to prove that the system can well perform the two objectives, fine position and torque tracking under arbitrary time-varying delays.

Theorem 1. Consider the system (27) with the control laws (35) in the absence of the human and environmental torques ($\tau_h(t) = \tau_e(t) = 0$). The position tracking errors defined in (16) can be driven onto the sliding mode surface and converge to zero in finite time under time-varying delays.

Consider a positive definite function V_1 for the system as:

$$V_1 = \sum_{i=m1,m2,s1,s2} \frac{1}{2} e_i^T C_i e_i \tag{37}$$

$\dot{V}_1$ can be derived as

$$\dot{V}_1 = -\sum_i e_i^T b_{i1} sig^{2-\varphi_3}(s_i) - \sum_i e_i^T b_{i2} sig^{\varphi_3}(s_i) - \sum_i e_i^T \frac{b_{i3}}{2} e_i + \sum_i e_i^T \phi \Gamma_i sign(e_i) k_{i3}^{2-\varphi_3} \left| e_{vi}^{\varphi_3(2-\varphi_3)} \right| + \sum_i e_i^T \phi \Gamma_i sign(e_i) k_{i3}^{\varphi_3} \left| e_{vi}^{\varphi_3^2} \right| + \sum_i e_i^T (G_i - \hat{G}_i) \tag{38}$$

As analysed before, the state estimator designed in (29) allows $\hat{G}_i$ fast tracks G_i to the extent that $\sum_i e_i^T (G_i - \hat{G}_i)$ in (38) is neighbouring zero and can be ignored. Knowing that

$$-e_i^T b_{i1} sig^{2-\varphi_3}(s_i) = b_{i1} \left(-k_{i1} (\|e_i\|^2)^{\frac{1}{2(2-\varphi_3)} + \frac{\varphi_1}{2}} - k_{i2} (\|e_i\|^2)^{\frac{1}{2(2-\varphi_3)} + \frac{\varphi_2}{2}} - e_i^{\frac{1}{2-\varphi_3}} * k_{i3} (e_{vi})^{\varphi_3} \right)^{2-\varphi_3}$$

when $sign(e_i) sign(e_{vi}) \geq 0$, we derive $-e_i^{\frac{1}{2-\varphi_3}} * k_{i3} (e_{vi})^{\varphi_3} \leq 0$. Therefore

$$-e_i^T b_{i1} sig^{2-\varphi_3}(s_i) \leq -b_{i1} \left(k_{i1} (\|e_i\|^2)^{\frac{1}{2(2-\varphi_3)} + \frac{\varphi_1}{2}} + k_{i2} (\|e_i\|^2)^{\frac{1}{2(2-\varphi_3)} + \frac{\varphi_2}{2}} \right)^{2-\varphi_3}$$

$$\leq -\frac{1}{2} b_{i1} k_{i1}^{2-\varphi_3} \|e_i\|^{1+\varphi_1(2-\varphi_3)} - \frac{1}{2} b_{i1} k_{i2}^{2-\varphi_3} \|e_i\|^{1+\varphi_2(2-\varphi_3)} \tag{39}$$

Also, when $sign(e_i) sign(e_{vi}) \geq 0$, $\Gamma_i = -1 \ or \ 0$ that makes $\sum_i e_i^T \phi \Gamma_i sign(e_i) k_{i3}^{2-\varphi_3} \left| e_{vi}^{\varphi_3(2-\varphi_3)} \right| + \sum_i e_i^T \phi \Gamma_i sign(e_i) k_{i3}^{\varphi_3} \left| e_{vi}^{\varphi_3^2} \right|$ no more than zero. Similarly,

$$-e_i^T b_{i2} sig^{\varphi_3}(s_i) \leq -b_{i2} \left(k_{i1} (\|e_i\|^2)^{\frac{1}{2\varphi_3} + \frac{\varphi_1}{2}} + k_{i2} (\|e_i\|^2)^{\frac{1}{2\varphi_3} + \frac{\varphi_2}{2}} \right)^{\varphi_3}$$

$$\leq -\frac{1}{2} b_{i2} k_{i1}^{\varphi_3} \|e_i\|^{1+\varphi_1 \varphi_3} - \frac{1}{2} b_{i2} k_{i2}^{\varphi_3} \|e_i\|^{1+\varphi_2 \varphi_3} \tag{40}$$

Based on (39)-(40), we derive

$$\dot{V}_1 \leq \sum_i \{ -\frac{1}{2} b_{i1} k_{i1}^{2-\varphi_3} \|e_i\|^{1+\varphi_1(2-\varphi_3)} - \frac{1}{2} b_{i1} k_{i2}^{2-\varphi_3} \|e_i\|^{1+\varphi_2(2-\varphi_3)} - \frac{1}{2} b_{i2} k_{i1}^{\varphi_3} \|e_i\|^{1+\varphi_1 \varphi_3} - \frac{1}{2} b_{i2} k_{i2}^{\varphi_3} \|e_i\|^{1+\varphi_2 \varphi_3} \}$$

$$= \sum_i \{ -\frac{1}{2} (2C_i^{-1})^{\frac{1+\varphi_1(2-\varphi_3)}{2}} b_{i1} k_{i1} \left(\frac{1}{2} e_i^T C_i e_i \right)^{\frac{1+\varphi_1(2-\varphi_3)}{2}} - \frac{1}{2} (2C_i^{-1})^{\frac{1+\varphi_2(2-\varphi_3)}{2}} b_{i1} k_{i2} \left(\frac{1}{2} e_i^T C_i e_i \right)^{\frac{1+\varphi_2(2-\varphi_3)}{2}} - \frac{1}{2} (2C_i^{-1})^{\frac{1+\varphi_1 \varphi_3}{2}} b_{i2} k_{i1} \left(\frac{1}{2} e_i^T C_i e_i \right)^{\frac{1+\varphi_1 \varphi_3}{2}} - \frac{1}{2} (2C_i^{-1})^{\frac{1+\varphi_2 \varphi_3}{2}} b_{i2} k_{i2} \left(\frac{1}{2} e_i^T C_i e_i \right)^{\frac{1+\varphi_2 \varphi_3}{2}} \}$$

$$\leq -\Phi_1 V_1^{\delta_1} - \Phi_2 V_1^{\delta_2} - \Phi_3 V_1^{\delta_3} - \Phi_4 V_1^{\delta_4} \tag{41}$$

where $\Phi_1 = \lambda_{min} (\sum_i \frac{1}{2} (2C_i^{-1})^{\frac{1+\varphi_1(2-\varphi_3)}{2}} b_{i1} k_{i1})$, $\Phi_2 = \lambda_{min} (\sum_i \frac{1}{2} (2C_i^{-1})^{\frac{1+\varphi_2(2-\varphi_3)}{2}} b_{i1} k_{i2})$, $\Phi_3 = \lambda_{min} (\sum_i \frac{1}{2} (2C_i^{-1})^{\frac{1+\varphi_1 \varphi_3}{2}} b_{i2} k_{i1})$, $\Phi_4 = \lambda_{min} (\sum_i \frac{1}{2} (2C_i^{-1})^{\frac{1+\varphi_2 \varphi_3}{2}} b_{i2} k_{i2})$; and $\delta_1 = \frac{1+\varphi_1(2-\varphi_3)}{2}$, $\delta_2 = \frac{1+\varphi_2(2-\varphi_3)}{2}$, $\delta_3 = \frac{1+\varphi_1 \varphi_3}{2}$, $\delta_4 = \frac{1+\varphi_2 \varphi_3}{2}$. Extending **Lemma 2**, the reaching time can be derived as

$$T_r < \frac{1}{\Phi_1} \frac{2}{|\delta_1 - 1|} + \frac{1}{\Phi_2} \frac{2}{|\delta_2 - 1|} + \frac{1}{\Phi_3} \frac{2}{|\delta_3 - 1|} + \frac{1}{\Phi_4} \frac{2}{|\delta_4 - 1|}$$

which means the overall system can remain stable in a finite time.

when $sign(e_i) sign(e_{vi}) < 0$, we derive $-e_i^{\frac{1}{2-\varphi_3}} * k_{i3} (e_{vi})^{\varphi_3} > 0$. Then, $-e_i^T b_{i1} sig^{2-\varphi_3}(s_i) < b_{i1} \left| e_i^{\frac{1}{2-\varphi_3}} * k_{i3} (e_{vi})^{\varphi_3} \right|^{2-\varphi_3}$ and $-e_i^T b_{i2} sig^{\varphi_3}(s_i) < b_{i2} \left| e_i^{\frac{1}{\varphi_3}} * k_{i3} (e_{vi})^{\varphi_3} \right|^{\varphi_3}$ Under this condition Γ_i satisfies $\Gamma_i = 1$ that makes $e_i^T \phi \Gamma_i sign(e_i) k_{i3}^{2-\varphi_3} \left| e_{vi}^{\varphi_3(2-\varphi_3)} \right|$ to be $-\phi \left| e_i^{\frac{1}{2-\varphi_3}} * k_{i3} (e_{vi})^{\varphi_3} \right|^{2-\varphi_3}$, and $e_i^T \phi \Gamma_i sign(e_i) k_{i3}^{\varphi_3} \left| e_{vi}^{\varphi_3^2} \right|$ to be $-\phi \left| e_i^{\frac{1}{\varphi_3}} * k_{i3} (e_{vi})^{\varphi_3} \right|^{\varphi_3}$. By setting $\phi \geq b_{i1}$ and $\phi \geq b_{i2}$, $\dot{V}_1$ is also guaranteed to be non-positive. The overall system stability can be guaranteed during free space motion. The proof is complete.

Theorem 2. When involving the human and the environmental forces, the system (27) with the control laws (35) can still remain stable and the torque tracking errors can converge to zero at the steady state during time-varying delays.

Consider a positive definite function V_2 for the system as:

$$V_2 = V_1 + \sum_i \frac{1}{2} y_i^T y_i \tag{42}$$

Based on (25), $\dot{V}_2$ is derived as

$$\dot{V}_2 = \dot{V}_1 - \sum_i e_i^T e_i + \sum_i e_i^T b_{i3} |z_i| \epsilon_i - \sum_i e_i^T b_{i4} z_i - \sum_i y_i^T p_{i1} (sig^{2\varphi_1 - 1}(y_i) + sig^{2\varphi_2 - 1}(y_i)) - \sum_i y_i^T p_{i2} \kappa_i \epsilon_i$$

$$\leq -\sum_i (p_{i1} - b_{i3}^2 h_i^2 - b_{i4}^2) \|y_i\|^{2\varphi_1} - \sum_i (p_{i1} - b_{i3}^2 h_i^2 - b_{i4}^2) \|y_i\|^{2\varphi_2} - \sum_i y_i^T p_{i2} \kappa_i \epsilon_i$$

$$\leq -\Upsilon V_2^{\varphi_1} - \Upsilon V_2^{\varphi_2} \tag{43}$$

where $\Upsilon = 2(p_{i1} - b_{i3}^2 h_i^2 - b_{i4}^2)$ Based on (26), the term $-\sum_i y_i^T p_{i2} \kappa_i \epsilon_i$ is always non-positive. Therefore, by setting $p_{i1} \geq b_{i3}^2 h_i^2 + b_{i4}^2$, $\dot{V}_2$ can be guaranteed to be negative, and y_i belongs to L_2 space that makes the force/torque tracking errors fast converge to zero in the finite time. The reaching time can be derived from (43) as

$$T_r < \frac{1}{\Upsilon} \frac{1}{\varphi_1 - 1} + \frac{1}{\Upsilon} \frac{1}{1 - \varpi_1}$$

This completes the proof.

6. Experiment

In this section, a series of experiments are carried out to validate the effectiveness of the proposed multilateral teleoperation system. Interval Type-2 T-S fuzzy models are constructed to describe the dynamics for master and slave robots. Due to the limit of pages, only the results of slave 1 is presented. The sampling time interval is 1ms, the number of data samples is 10700, and the number of fuzzy sets/rules is determined as nine. As shown in Fig. 6, compared to Type-1 fuzzy model, Type-2 fuzzy model achieves greatly reduced RMSE. Especially, for the samples from no. 9500 to 10700 where the measured outputs are zero, the Type-1 fuzzy model's output cannot settle at zero while Type-2 fuzzy model's outputs can exactly track the measured signals.
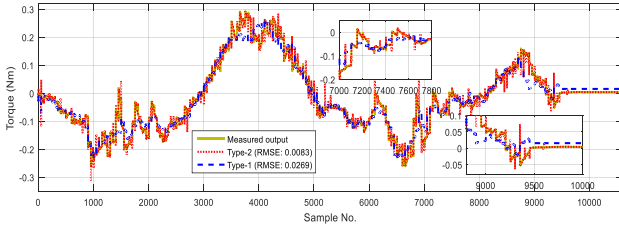

Fig. 6. Accuracy evaluation of the proposed Type-2 fuzzy model

For the NFTSM surface of the cooperative structure, the parameters are determined as $k_{i1} = k_{i2} = 1$, $k_{i3} = 0.1$. $\varphi_1 = \frac{l_1}{p} = \frac{15}{7}$, $\varphi_3 = \frac{l_2}{p} = \frac{9}{7}$. In φ_2, $\varpi_1 = 17/19$, $\varpi_2 = 3$. For the dominance factor, $\alpha = 25$. For the force control, $c_{s11} = c_{s21} = 0.5$, $c_{s12} = c_{s22} = 0.1$, $c_{m11} = c_{m21} = 1$, $c_{m12} = c_{m22} = 0.15$. $p_{i1} = 10$, $p_{i2} = 3$. For zero drift compensator, $\eth_{i1} = 10$, $\eth_{i2} = 50$, $\eth_{i3} = 30$. For the state observers, $\beta_{i1} = 100$, $\beta_{i2} = 10$, $\beta_{i3} = 0.2$. $A_{i0} = 1$, $A_{i\infty} = 0.05$, $\iota = 0.1$. C_i, D_i, E_i are the derived from fuzzy models. For the main control laws, $b_{s11} = b_{s21} = 1$, $b_{s12} = b_{s22} = 5$, and $b_{m11} = b_{m21} = 0.5$, $b_{m12} = b_{m22} = 2$. $\phi = 5$. $b_{s13} = b_{s23} = 1$, $b_{m13} = b_{m23} = 2$, $b_{i4} = 1$.
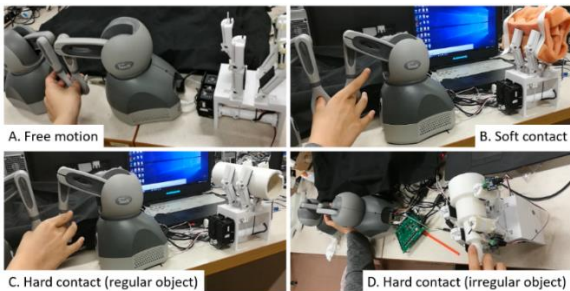

Fig. 7. A. Free motion; B. Soft contact; C. Hard contact (regular object); D. Hard contact irregular object

At the slave sides, each gripper attaches one Flexiforce pressure sensor to measure the environmental contact force. At the master sides, since adding force sensors may interfere human operating the manipulators, the force observer proposed in [41], which uses the extended Kalman filter to suppress external noises, is applied to the haptic devices in order to estimate the human force, and Type-2 fuzzy model is used to replace the mathematical dynamic function for this force observer design.

As an underactuated robot hand, its exact kinematics is hard to derive on-line. Therefore, the kinematics of the teleoperation system is ignored in this paper. Besides, for simplicity, we assume the measured environmental force is proportional to the environmental torque with a known constant gain. The time delays are approximately 400ms with 100ms variation.

A. Free Motion

In the experiment of free motion, the two master haptic devices drive the slave grippers which do not contact any environmental objects as shown in Fig. 7A. It should be noted that no matter whether the system is in free motion or contacting objects, the motors of the robot hand need to keep dragging the fingers, and thus are always loaded.

The aim of this free motion experiment is to make the slave grippers closely track the motion of the master haptic devices and meanwhile, the operator at the master side does not feel large feedback force so that he/she can fluently drive the master devices. The uncertainty caused by the internal forces, such as the frictions of the components in the robot hand, is the main issue that can adversely affect the masters-slaves motion convergence and simultaneously increase the force feedback to the masters.
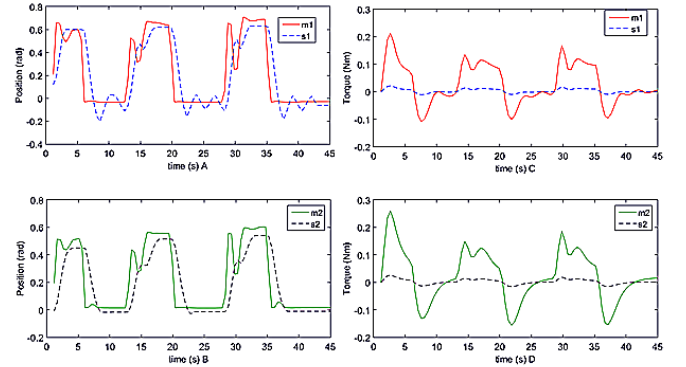

Fig. 8. Position and force tracking (free motion [27]); $q_{m1} \leftrightarrow q_{s1}$; $q_{m2} \leftrightarrow q_{s2}$; $\tau'_{h1} \leftrightarrow \tau'_{e1}$; $\tau'_{h2} \leftrightarrow \tau'_{e2}$

Table 1. RMSE (tracking errors for Fig. 8)

RMSE	Position	Torque
m1 − s1	0.3181	0.5951
m2 − s2	0.2993	0.5273

Fig. 8 shows the position and torque tracking performance of the system in [27]. The system in [27] uses the controllers containing the force errors between master and slave using force observers in order to improve the human perception on the environment. However, using only PD control method, finite-time position convergence is unable to derive and large position variations and errors occur at the steady state (10-13s, 21-25s, 34-39s). Also, the system uncertainties mainly containing internal forces impede the slaves (fingers) to track

the masters' positions (3-6s, 15-20s, 30-35s). furthermore, the force observer applied in [27] highly depends on exact dynamic model. Without the mathematical dynamic model, the estimated torques are not accurate that together with the system uncertainty let the operator feel large feedback force during free motion (larger than 0.2 Nm).

Fig. 9 shows the position and torque tracking performance of the system in [42]. By using the NFTSM, the position tracking does not does not contain large variation and errors. Finite time convergence can be achieved. However, because of the large but unknown mass of the slave grippers and the time delay, a certain time is still required in order to allow the slaves to accurately track the masters. As analysed before, the conventional Mamdani fuzzy logic used in [42] has poor performance on uncertainties tracking and estimation. Thus, the system uncertainties also influence the performance of this system. In addition, without force control algorithms, the large position control gains can seriously interrupt the operator's feeling about the remote environment. Therefore, large feedback force is still derived in the master side (larger than 0.2 Nm).
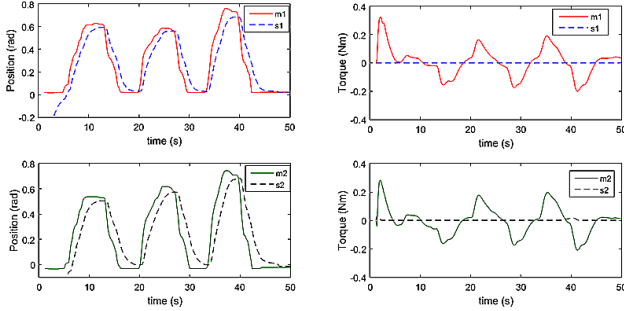

Fig. 9. Position and force tracking (free motion [42]); $q_{m1} \leftrightarrow q_{s1}$; $q_{m2} \leftrightarrow q_{s2}$; $\tau'_{h1} \leftrightarrow \tau'_{e1}$; $\tau'_{h2} \leftrightarrow \tau'_{e2}$

Table 2. RMSE (tracking errors for Fig. 9)

RMSE	Position	Torque
m1 – s1	0.2395	0.4703
m2 – s2	0.2480	0.4937

The position and force tracking of the proposed system are shown as Fig. 10. When the two masters move to the same position, the two slave grippers can fast track their motion without large overshoot or variations, and the tracking errors are zero at the steady state. Compared with Fig. 9, the proposed NFTSM has faster convergence performance. Also, since the end effectors of the slave grippers do not contact to any object, the outputs of the sensors are zero. With compensation for the system uncertainties and accurate force tracking strategy, the human operator does not feel feedback force and the applied human force is also neighbouring to zero.
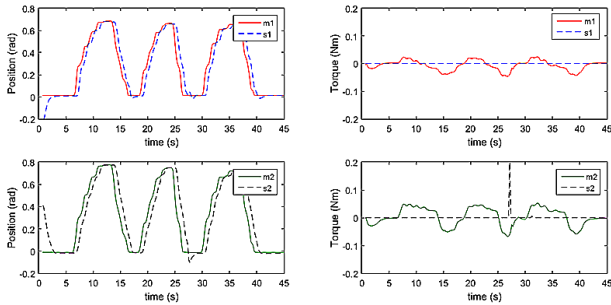

Fig. 10. Position and force tracking (free motion, our system); $q_{m1} \leftrightarrow q_{s1}$; $q_{m2} \leftrightarrow q_{s2}$; $\tau'_{h1} \leftrightarrow \tau'_{e1}$; $\tau'_{h2} \leftrightarrow \tau'_{e2}$

Table 3. RMSE (tracking errors for Fig. 9)

RMSE	Position	Torque
m1 – s1	0.0297	0.1063
m2 – s2	0.0301	0.1194

B. Soft contact

In this experiment, the slave grippers are controlled to grasping a soft sponge as shown in Fig. 7B. When contacting the soft sponge, the grippers continue moving to squeeze the sponge until their motions stop (the soft contact turns to hard contact).
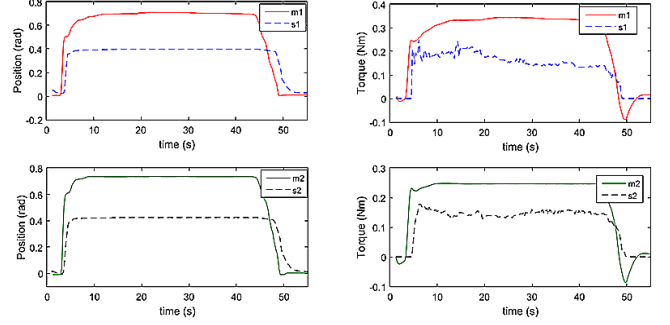

Fig. 11. Position and force tracking (soft contact [34]); $q_{m1} \leftrightarrow q_{s1}$; $q_{m2} \leftrightarrow q_{s2}$; $\tau'_{h1} \leftrightarrow \tau'_{e1}$; $\tau'_{h2} \leftrightarrow \tau'_{e2}$

Table 4. RMSE (tracking errors for Fig. 11)

RMSE	Position	Torque
m1 – s1	1.9832	0.8438
m2 – s2	2.0731	0.7953

Fig. 11 shows the position and force tracking of the system in [34]. The system in [34] uses the designed auxiliary filter to improve the position tracking ability. Without force tracking control algorithms, the operator can hardly adjust the force of the slave grippers. Therefore, the operator has to largely move the master manipulators so that the large position errors can enhance the remote slaves' contact force to grasp the soft sponge tightly. When the slave holding the sponge tightly, the position errors largely increase the feedback force so that the operator has to exert extra forces in order to provide the slave enough force to grasp the sponge.

Fig. 12 shows the position and force tracking of our system. From 8th second, the grippers start to contact to the soft sponge and the operator's torques of the two master haptic devices increase from 0 Nm to 0.4 Nm. The environmental torques also track the operator's. The signals of the measured environmental torques are fed back to the master sides so that the masters adaptively adjust their positions to converge to the position of the slaves. When the operator stops exerting force, the operator's and environmental torques directly converge to zero and the master and slave positions return to zero.
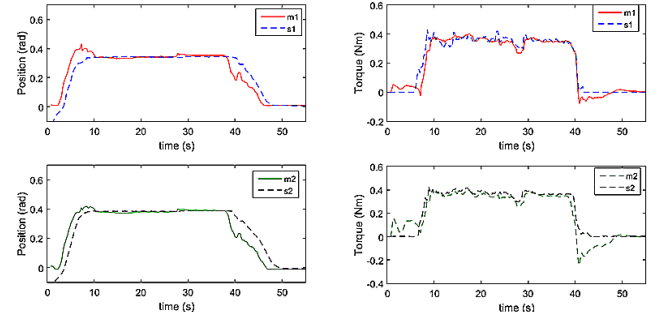

Fig. 12. Position and force tracking (soft contact, our system); $q_{m1} \leftrightarrow q_{s1}$; $q_{m2} \leftrightarrow q_{s2}$; $\tau'_{h1} \leftrightarrow \tau'_{e1}$; $\tau'_{h2} \leftrightarrow \tau'_{e2}$

Table 5. RMSE (tracking errors for Fig. 12)

RMSE	Position	Torque
m1 – s1	0.0337	0.0219
m2 – s2	0.0309	0.0408

C. Hard Contact (regularly-shaped object)

In this experiment, the slave grippers are controlled to contact to a solid cylinder as shown in Fig. 7C. when contacting to a solid object, the masters need to directly derive the feedback force signals so that the operator feels a large feedback and hardly goes on the motion.
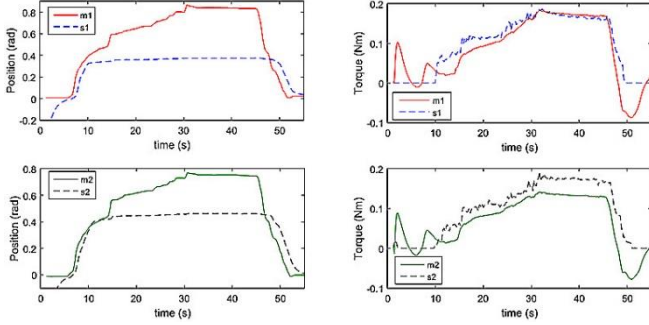

Fig. 13. Position and force tracking (regularly-shaped object [33]); $q_{m1} \leftrightarrow q_{s1}$; $q_{m2} \leftrightarrow q_{s2}$; $\tau'_{h1} \leftrightarrow \tau'_{e1}$; $\tau'_{h2} \leftrightarrow \tau'_{e2}$

Table 6. RMSE (tracking errors for Fig. 13)

RMSE	Position	Torque
m1 – s1	2.1735	0.3671
m2 – s2	2.0943	1.4752

Fig. 13 shows the position and force tracking performances of the system in [33] when contacting to the regularly-shaped object. The system in [33] utilizes a robust control algorithm to guarantee the delay-based stability for multilateral teleoperation system. Mamdani fuzzy models are also applied in this system to deal with uncertainties. Similar with the system in [34], the system in [33] also does not have a good force control algorithm so that the operator has to enlarge the position tracking errors in order to enlarge the environmental torque to hold the solid object tightly. Although fine torque tracking is achieved, the masters' positions are basically twice as large as the slave's positions at the steady state.
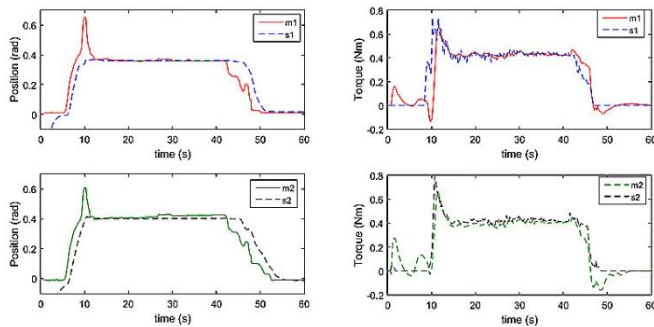

Fig. 14. Position and force tracking (regularly-shaped object, our system); $q_{m1} \leftrightarrow q_{s1}$; $q_{m2} \leftrightarrow q_{s2}$; $\tau'_{h1} \leftrightarrow \tau'_{e1}$; $\tau'_{h2} \leftrightarrow \tau'_{e2}$

Table 7. RMSE (tracking errors for Fig. 14)

RMSE	Position	Torque
m1 – s1	0.0487	0.0391
m2 – s2	0.0471	0.0373

Fig. 14 shows the position and force tracking performances of our system when contacting to the regularly-shaped object. When firstly contact to the solid object, the environmental

torques jump to around 0.6 Nm. Then the master haptic devices directly receive large force feedback so that they fast adjust their positions to track the slaves' position. When the position synchronization is derived during the hard contact, the contact torques of the master haptic devices and the slave grippers decrease to around 0.4 Nm. The proposed force controllers allow the operator's forces to closely track the environmental forces. Therefore, the torque tracking errors are neighbouring to zero. Besides, the large feedback force also impedes the masters' motion to the extent that basically no position tracking errors occur at the steady state during hard contact. When the operator relaxes the force, all the position and torque signals fast back to zero.

Moreover, based on the proposed control algorithms, master 1 and master 2 can freely drive slave 1 and slave 2, respectively. Since the two slave gripers are treated as an integral slave robot, the mixed position and force information adjusted by the varying dominance factors is fed back to the two masters to allow they receive same perception on the integrate slave hand. Thus, the operator(s) can feel the same feedback force from master 1 and master 2. Therefore, from Figs. 10 and 12, the human applied forces and the masters' positions of master 1 and master 2 are basically the same.

D. Hard Contact (irregularly-shaped object)

The proposed system is expected to allow the operator(s) to equally drive the two masters to reach a designated point and consequently control the two slave grippers to tightly hold the objects with different texture and different shape (even with the irregular shape). Without the mutual control between the two slave grippers, they cannot adjust the force to hold the irregularly-shaped object. Therefore, all the above systems used for comparison are not suitable for this experiment, while the proposed system can give satisfactory performance as shown in Fig. 7D, where the slave grippers are controlled to hold an irregular-shaped object, and the position as well as torque tracking are shown in Fig. 15.
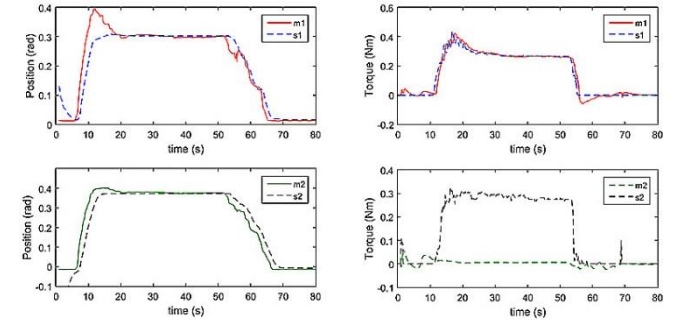

Fig. 15. Position and force tracking (irregularly-shaped object, our system); $q_{m1} \leftrightarrow q_{s1}$; $q_{m2} \leftrightarrow q_{s2}$; $\tau'_{h1} \leftrightarrow \tau'_{e1}$; $\tau'_{h2} \leftrightarrow \tau'_{e2}$

Table 8. RMSE (tracking errors for Fig. 15)

RMSE	Position	Torque
m1 – s1	0.0520	0.0292
m2 – s2	0.0484	0.4048

Firstly, when driving the two masters to conduct the same motion, slave 1 firstly contacts to the object. Due to its irregular shape, slave 2 does not contact the object. Then, according to the control algorithm in (35), slave 1 feeds the environmental force back to the masters and slave 2 so that slave 2 follows the force information from slave 1 to go on moving to contact to the object and then applies the same force

as that of slave 1. At the steady state, the environmental torques of masters 1 and 2, slaves 1 and 2 maintain at around 0.3 Nm. The position signals of slaves are also fed back to the master side in order to allow the masters to closely track the motion of slaves.

E. Dealing with varying zero drift

Since force control is an important part of the proposed system, the exist varying zero drift in force sensors/observers problem is a main issue that may seriously affect the operator feeling the remote environment. The operator may still feel force feedback even all of the robots stop their motion because of the zero drift. By using the proposed sliding mode control algorithm in (24)-(25), the measured torque signals can remain zero when the no human or environmental force is exerted into the system as shown in Fig. 16.
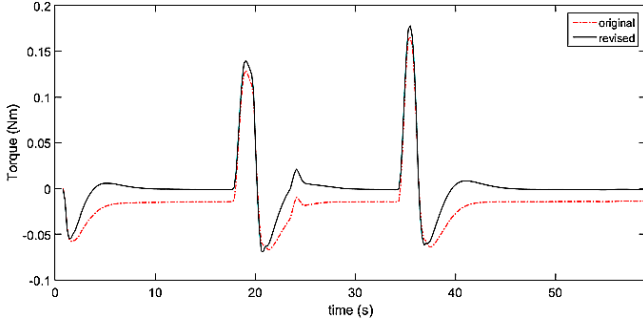

Fig. 16. Original and revised torque signals; $\tau'_{h1} \leftrightarrow \tau'_{e1}$

F. Performance of the fuzzy model-based state observer

As analysed before, in the fuzzy model-based state observer in (29), the close tracking between Y_{i1} and Z_i determines the close tracking between Y_{i2} and Z_i^*. That is, the unknown dynamic uncertainties can be estimated and compensated for by the state observer. Fig. 17 demonstrate the close tracking between Y_{s11} and Z_{s1} by using (29) to suppress the errors in a small region. The RMSE between Y_{s11} and Z_{s1} is 0.0103. Therefore, it can be concluded that the dynamic uncertainties can be compensated by the proposed state observer.
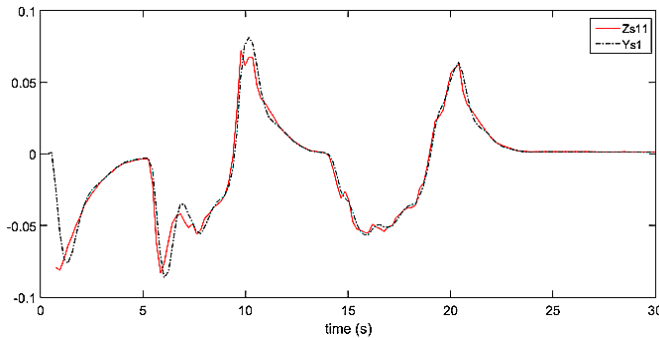

Fig. 17. Y_{s11} and Z_{s1} in our system

The proposed state observer is an extension of the state observer in [40]. There are two unsolved problems of the state observer in [40]. Firstly, only the errors between Y_{i1} and Z_i with a constant gain are applied in the state observer. When the slave robot hand is conducting motions such as free motions and holding environmental object, Y_{i1} cannot fastly track Z_i as shown as Fig. 18. The RMSE between Y_{s11} and Z_{s1} is 0.5817. Therefore, the changing Z_i^* can also not accurately tracked by Y_{i2}. Moreover, the state observer in [40] still depends on the pre-knowledge of the mathematical dynamics of the systems, which is unachievable for the slave robot hand.
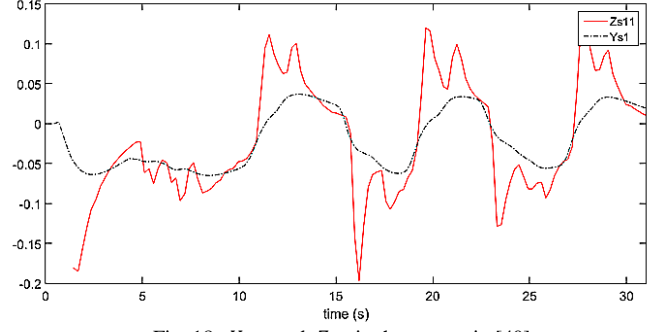

Fig. 18. Y_{s11} and Z_{s1} in the system in [40]

Fig.19 shows multiple real applications of the designed gripper, which are Grasping raw eggs, Hand shaking, Grasping a bread, Grasping a 1.5 litre bottle, Grasping four pieces of tofu, Grasping a pen to write and Grasping a bunch of bananas.
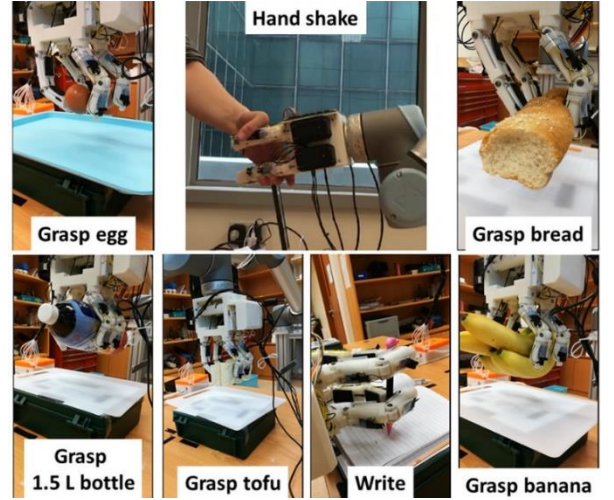

Fig. 19. Multiple real applications of the designed gripper

7. Conclusion

In this paper, we present a new multilateral tele-manipulated robot hand control system. In the slave side, a multi-fingered robot hand is built containing two gripers. With the cooperation of the two gripers, objects with different shapes can be tightly grasped. In the master side, two haptic devices are applied to collaboratively control the remote robot hand. A developed NFTSM method with varying dominance factor is proposed to provide the system fast position and force tracking ability and meanwhile allow the operator to have a mixed feeling on the remote environment. Type-2 Fuzzy Logic algorithm is applied to model the overall system dynamics and a fuzzy-based state observer is also proposed to compensate for system uncertainties. To deal with the zero drift of the force observers and force sensors, a new sliding mode adaptive controller is also designed in this paper. The experiment results demonstrate the superiority of the proposed system. In the future work, more DOF will be added for the designed multi-fingered robot hand in order to further improve its flexibility. Estimation and application of the kinematics of the proposed robot hand will also be considered.

Reference:

[1] Butterfaß, Jörg, et al. "DLR-Hand II: Next generation of a dextrous robot hand." Robotics and Automation, 2001. Proceedings 2001 ICRA. IEEE International Conference on. Vol. 1. IEEE, 2001.

[2] Rothling, Frank, et al. "Platform portable anthropomorphic grasping with the bielefeld 20-dof shadow and 9-dof tum hand." Intelligent Robots and Systems, 2007. IROS 2007. IEEE/RSJ International Conference on. IEEE, 2007.

[3] Morrow, John, et al. "Improving Soft Pneumatic Actuator fingers through integration of soft sensors, position and force control, and rigid fingernails." Robotics and Automation (ICRA), 2016 IEEE International Conference on. IEEE, 2016.

[4] Deimel, Raphael, and Oliver Brock. "A novel type of compliant and underactuated robotic hand for dexterous grasping." The International Journal of Robotics Research 35.1-3 (2016): 161-185.

[5] Dollar, Aaron M., and Robert D. Howe. "A robust compliant grasper via shape deposition manufacturing." IEEE/ASME transactions on mechatronics 11.2 (2006): 154-161.

[6] Odhner, Lael U., et al. "A compliant, underactuated hand for robust manipulation." The International Journal of Robotics Research 33.5 (2014): 736-752.

[7] V.I. Utkin. Sliding Modes in Control and Optimization. Communication and control engineering. Springer-Verlag, 1992.

[8] V.I. Utkin, J. Guldner, and J. Shi. Sliding Model Control in Electromechanical Systems. Taylor and Francis Ltd, 1999.

[9] C. Edwards and S. Spurgeon. Sliding Mode Control: Theory and Applications . Systems and Control. Taylor & Francis, 1998.

[10] Ferrara and G. P. Incremona. Design of an integral suboptimal second order sliding mode controller for the robust motion control of robot manipulators.

[11] G. P. Incremona, G. De Felici, A. Ferrara, and E. Bassi. A supervisory sliding mode control approach for cooperative robotic system of systems. IEEE Systems Journal, 9(1):263–272, Mar. 2015.

[12] S. T. Venkataraman and S. Gulati, "Control of nonlinear systems using terminal sliding modes," ASME J. Dyn. Syst. Meas. Control, vol. 115, pp. 554–560, Sep. 1993.

[13] F. B. Li, L. G. Wu, P. Shi, and C. C. Lim, "State estimation and sliding mode controller for semi-Markovian jump systems with mismatched uncertainties," Automatica, vol. 51, pp. 385–393, Jan. 2015.

[14] S. H. Yu, X. H. Yu, B. J. Shirinzadeh, and Z. H. Man, "Continuous finite-time control for robotic manipulators with terminal sliding mode," Automatica, vol. 41, no. 11, pp. 1957–1964, 2005.

[15] K. F. Lu and Y. Q. Xia, "Adaptive attitude tracking control for rigid spacecraft with finite-time convergence," Automatica, vol. 49, no. 12, pp. 3591–3599, 2013.

[16] Y. N. Yang, C. C. Hua, and X. P. Guan, "Adaptive fuzzy finite-time coordination control for networked nonlinear bilateral teleoperation system," IEEE Trans. Fuzzy Syst., vol. 22, no. 3, pp. 631–641, Jun. 2014.

[17] Y. N. Yang, C. C. Hua, and X. P. Guan, "Finite Time Control Design for Bilateral Teleoperation System With Position Synchronization Error Constrained", Vol.46, No.3, pp.609-609

[18] Hua, Changchun, et al. "Extended-state-observer-based finite-time synchronization control design of teleoperation with experimental validation." Nonlinear Dynamics (2016): 1-15.

[19] Suzuki, Atsushi, and Kouhei Ohnishi. "Frequency-domain damping design for time-delayed bilateral teleoperation system based on modal space analysis." IEEE Transactions on Industrial Electronics 60.1 (2013): 177-190.

[20] Hashtrudi-Zaad, Keyvan, and Septimiu E. Salcudean. "Transparency in time-delayed systems and the effect of local force feedback for transparent teleoperation." IEEE Transactions on Robotics and Automation 18.1 (2002): 108-114.

[21] Aziminejad, A., Tavakoli, M., Patel, R. V., & Moallem, M. (2008). Transparent time-delayed bilateral teleoperation using wave variables. IEEE Transactions on Control Systems Technology, 16(3), 548-555.

[22] Chawda, V.; OMalley, M.K., "Position Synchronization in Bilateral Teleoperation Under Time-Varying Communication Delays," Mechatronics, IEEE/ASME Transactions on , vol.20, no.1, pp.245,253, Feb. 2015.

[23] Ganjefar, S., Rezaei, S., & Hashemzadeh, F. (2017). Position and force tracking in nonlinear teleoperation systems with sandwich linearity in actuators and time-varying delay. Mechanical Systems and Signal Processing, 86, 308-324.

[24] F. Hashemzadeh andM. Tavakoli, "Position and force tracking in nonlinear teleoperation systems under varying delays," Robotica, vol. 33, no. 4, pp.1–14, 2014.

[25] H. Amini,, B. Farzaneh, F. Azimifar, A.A.D. Sarhan. "Sensor-less force-reflecting macro–micro telemanipulation systems by piezoelectric actuators." ISA transactions Vol. 64, pp. 29 3-302, 2016.

[26] Azimifar, F., Hassani, K., Saveh, A. H., & Tabatabai Ghomshe, F. (2017). Performance analysis in delayed nonlinear bilateral teleoperation systems by force estimation algorithm. Transactions of the Institute of Measurement and Control, 0142331216688751.

[27] Azimifar, F., Abrishamkar, M., Farzaneh, B., Sarhan, A. A. D., & Amini, H. (2017). Improving teleoperation system performance in the presence of estimated external force. Robotics and Computer-Integrated Manufacturing,46, 86-93.

[28] L.X. Wang, J.M. "Mendel, Fuzzy basis functions, universal approximation, and orthogonal least-squares learning," IEEE Transactions on Neural Networks, No. 3 pp. 807-814, 1992.

[29] Y. Hao, "General SISO Takagi-Sugeno fuzzy systems with linear rule consequent are universal approximators," IEEE Transactions on Fuzzy Systems No. 6, pp. 582-587, 1998.

[30] K. Zeng, N. Y. Zhang, and W. L. Xu, "A comparative study on sufficient conditions for takagi–sugeno fuzzy systems as universal approximators," IEEE Transactions on Fuzzy Systems, Vol. 8, No. 6, pp. 773-780, 2000.

[31] G. Feng, "A survey on analysis and design of model-based fuzzy control systems," IEEE Transactions on Fuzzy Systems, Vol. 14, No. 5, pp. 676-697, 2006.

[32] Y. Yang, C. Huan, and X. Guan, Adaptive fuzzy synchronization control for networked teleoperation system with input and multi-state constraints, Journal of the Franklin Institute, Vol. 353, pp. 2814-2834, 2016.

[33] Z. Li, Y. Xia and F. Sun, "Adaptive fuzzy control for multilateral cooperative teleoperation of multiple robotic manipulators under random network-induced delays," IEEE Transactions on Fuzzy Systems, Vol. 22, No. 2, 2014.

[34] D.H. Zhai, Y. Xia, "Adaptive Fuzzy Control of Multilateral Asymmetric Teleoperation for Coordinated Multiple Mobile Manipulators," IEEE Transactions on Fuzzy Systems, Vol. 24, No. 1, 2016.

[35] Q.L. Liang, J.M. Mendel, "An introduction to type-2 TSK fuzzy logic systems." IEEE International Fuzzy Systems. Conference Proceedings, Seoul, South Korea, 1999, pp. 1534-1539.

[36] D. E. Gustafson, W. C. Kessel, "Fuzzy clustering with a fuzzy covariance matrix." IEEE Conference on Decision and Control including the 17th Symposium on Adaptive Processes, San Diego, USA, 1978, pp. 761-766.

[37] J. M. Mendel, "Computing Derivatives in Interval Type-2 Fuzzy Logic Systems." IEEE Transactions on Fuzzy Systems, 12 (1), pp. 84-98, 2004

[38] Yang, L., & Yang, J. (2011). Nonsingular fast terminal sliding-mode control for nonlinear dynamical systems. International Journal of Robust and Nonlinear Control, 21(16), 1865-1879.

[39] Y. N. Yang, C. C. Hua, and X. P. Guan, "Finite Time Control Design for Bilateral Teleoperation System With Position Synchronization Error Constrained", IEEE Transactions on Cybernetics, Vol.46, No.3, pp.609-619, 2016.

[40] Hua, Changchun, et al. "Extended-state-observer-based finite-time synchronization control design of teleoperation with experimental validation." Nonlinear Dynamics (2016): 1-15.

[41] L. Chan, F. Naghdy, and D. Stirling, "An improved extended active observer for adaptive control of a constrained motion," Journal of Intelligent and Robotic Systems, pp. 1-14, 2016.

[42] Yang, Y., Hua, C., & Guan, X. (2014). Adaptive fuzzy finite-time coordination control for networked nonlinear bilateral teleoperation system.IEEE Transactions on Fuzzy Systems, 22(3), 631-641.

[43] Khooban, M. H., Niknam, T., Blaabjerg, F., & Dehghani, M. (2016). Free chattering hybrid sliding mode control for a class of non-linear systems: electric vehicles as a case study. IET Science, Measurement & Technology, 10(7), 776-785.

[44] Khooban, M. H., Niknam, T., & Sha-Sadeghi, M. (2016). A time-varying general type-II fuzzy sliding mode controller for a class of nonlinear power systems. Journal of Intelligent & Fuzzy Systems, 30(5), 2927-2937.

[45] Shahsadeghi, M., Khooban, M. H., & Niknam, T. (2014). A robust and simple optimal type II fuzzy sliding mode control strategy for a class of nonlinear chaotic systems. Journal of Intelligent & Fuzzy Systems, 27(4), 1849-1859.

[46] Q. Liao, & D Sun. "Interaction measures for control configuration selection based on interval type-2 Takagi-Sugeno fuzzy model." IEEE Transactions on Fuzzy Systems, 2018.

[47] Khooban, M. H., Vafamand, N., Liaghat, A., & Dragicevic, T. (2017). An optimal general type-2 fuzzy controller for Urban Traffic Network. ISA transactions, 66, 335-343.

[48] Khooban, M. H., Niknam, T., & Sha-Sadeghi, M. (2016). Speed control of electrical vehicles: a time-varying proportional–integral controller-based type-2 fuzzy logic. IET Science, Measurement & Technology, 10(3), 185-192.

[49] Liao, Q. F., Sun, D., Cai, W. J., Li, S. Y., & Wang, Y. Y. (2017). Type-1 and Type-2 effective Takagi-Sugeno fuzzy models for decentralized control of multi-input-multi-output processes. Journal of Process Control, 52, 26-44.

[50] D. Sun, Q. Liao, & H. Ren, "Type-2 Fuzzy Modeling and Control for Bilateral Teleoperation System with Dynamic Uncertainties and Time-varying Delays." *IEEE Transactions on Industrial Electronics*, vol. 61, no. 1, pp.447-459, 2018.

[51] D. Sun, Q. Liao, & H. Ren, "Type-2 Fuzzy logic based time-delayed shared control in online-switching tele-operated and autonomous systems," *Robotics and Autonomous Systems,* 2018.

[52] D. Sun, F. Naghdy and H. Du, "Neural Network-Based Passivity Control of Teleoperation System Under Time-Varying Delays", *IEEE Transactions on Cybernetics*, 2016.

[53] D. Sun, F. Naghdy, and H. Du. "Wave-variable-based Passivity Control of Four-channel Nonlinear Bilateral Teleoperation System under Time Delays." *IEEE Transactions on Mechatronics*, Vol. 21, No. 1, pp. 238-253, 2016

[54] D. Sun, F. Naghdy, and H. Du. "Application of wave-variable control to bilateral teleoperation systems: A survey." *Annual Reviews in Control*, vol. *38* no. 1. pp.12-31, 2014.

[55] Liu, S., Liu, P. X., & El Saddik, A. (2014). A stochastic game approach to the security issue of networked control systems under jamming attacks. *Journal of the Franklin Institute*, *351*(9), 4570-4583.

[56] Ye, X., S. Liu, and P. X. Liu. "Modelling and stabilisation of networked control system with packet loss and time-varying delays." *IET control theory & applications* 4.6 (2010): 1094-1100.
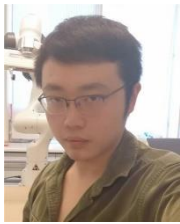
Da Sun received his B. Eng. and Ph. D. degrees in Mechatronics from University of Wollongong, Australia, 2012, and 2016, respectively. During 2016 -2017, he was a Research Fellow in National University of Singapore, Singapore. Currently, he is a Research Fellow in Örebro universitet, Sweden. His research interest includes Robotics, Control theory, Teleoperation and Virtual Reality.

Qianfang Liao received the B. Eng. degree in Automation from Wuhan University, Wuhan, China, in 2006, and the M. Eng. degree in Automation from Shanghai Jiao Tong University, Shanghai, China, in 2009, and Ph.D. degree from School of Electrical & Electronic Engineering, Nanyang Technological University, Singapore, in 2015. From 2015 to 2017, she was a Research Fellow in Nanyang Technological University and National University of Singapore. Currently, she is a Research Fellow in Örebro universitet, Sweden. Her research interests include fuzzy modelling and control for multivariable systems.

Xiaoyi Gu received the B.S. degree in mechanical engineering and automation from Shanghai Jiao Tong University, Shanghai, China, in 2013, and the M.E. degree from the department of biomedical engineering, national university of Singapore, Singapore, in 2015, where he is currently working toward the Ph.D degree. His current research interests include medical robots, bio-inspired robots, soft robots and smart actuators.

Changsheng Li received the B.S. and M.S. degrees in mechanical engineering from Harbin Engineering University, Harbin, China, in 2008 and 2011, respectively, and the Ph.D. degree in mechanical engineering from Beihang University, Beijing, China, in 2016.
Since 2016, he has been a Research Fellow with the Department of Biomedical Engineering, National University of Singapore. His research mainly focuses on medical robotics. His research interests include medical robotics and devices, robotic system design and mechanism analysis.

Hongliang Ren received his Ph.D. degree in electronic engineering (specialized in biomedical engineering) from The Chinese University of Hong Kong (CUHK), Shatin, Hong Kong, in 2008. He is currently an Assistant Professor and leading a research group on medical mechatronics in the Biomedical Engineering Department, National University of Singapore (NUS), Singapore. He is an affiliated Principal Investigator for the Singapore Institute of Neurotechnology (SINAPSE) and Advanced Robotics Center at the National University of Singapore. After his graduation, he was a Research Fellow at The Johns Hopkins University, Children's Hospital Boston and Harvard Medical School, and Children's National Medical Center, USA. His main research interests include biomedical mechatronics, magnetic actuation and sensing in medicine, computer-integrated surgery, and robotics in medicine.